INVESTIGATION OF HUMAN IL18 STRUCTURES TOWARDS UNDERSTANDING THE DYNAMICS AND SELF-ASSEMBLY OF IL18-IL18BP HETERODIMERS

A THESIS SUBMITTED TO

THE GRADUATE SCHOOL OF ENGINEERING AND SCIENCE

OF BILKENT UNIVERSITY

IN PARTIAL FULFILLMENT OF THE REQUIREMENTS FOR

THE DEGREE OF

MASTER OF SCIENCE

IN

MOLECULAR BIOLOGY AND GENETICS

BY

Yılmaz Yücehan Yazıcı

August 2023

To my family,

for always loving and supporting me

INVESTIGATION OF HUMAN IL18 STRUCTURES TOWARDS UNDERSTANDING THE DYNAMICS AND SELF-ASSEMBLY OF IL18-IL18BP HETERODIMERS

By Yılmaz Yücehan Yazıcı

August 2023

We certify that we have read this thesis and that in our opinion it is fully adequate, in scope and in quality, as a thesis for the degree of Master of Science.

Serkan Belkaya (Advisor)

Emel Timuçin (Co-Advisor)

Ilyas Chachoua

Perinur Bozaykut Eker

Approved for the Graduate School of Engineering and Science:

Orhan Arıkan

Director of the Graduate School of Engineering and Science

ABSTRACT

INVESTIGATION OF HUMAN IL18 STRUCTURES TOWARDS UNDERSTANDING THE DYNAMICS AND SELF-ASSEMBLY OF IL18-IL18BP HETERODIMERS

Yılmaz Yücehan Yazıcı
M.Sc. in Molecular Biology and Genetics
Advisor: Serkan Belkaya
Co-advisor: Emel Timuçin
August 2023

Interleukin-18 (IL18) is an inflammatory cytokine involved in the regulation of both innate and adaptive immunity. IL18 activity is tightly regulated by its constitutively secreted inhibitor, IL18 binding protein (IL18BP). All known IL18BPs from human to poxviruses share an identical protein fold. Investigation of known crystal structures of human IL18 illustrated that the region between the 68^{th} and 81^{st} amino acids is either missing or disordered in all IL18-IL18BP complexes while adopting a 3_{10} helical structure in the free or signaling complexes of IL18. The C74 residue in this region was reported to form a novel intermolecular disulfide bond in the human IL18-IL18BP tetrameric assembly. Yet, the impact of this small surface epitope on the stability and self-assembly of IL18 is unclear. First, we investigated the dynamics of this small surface region of IL18-IL18BP heterodimers by molecular dynamics simulations. In simulations, we used all known crystal structures of IL18-IL18BP and two additional computer models generated by AlphaFold2 and homology modeling to observe the differential folding of small surface regions. Next, we generated the proposed human and Yaba-like disease virus tetramers

and analyzed them with or without intermolecular disulfide bonds. We found that the helical structure of small surfaces stabilizes the backbone of the complex through reducing its flexibility. While our computational model folded into a more stable and less flexible short IL18 epitope, similar to free IL18 or bound IL18 on the signal complex, IL18 from the complexes with human or virus IL18BPs displayed flexible regions with a less stable backbone. The core of the human crystal loosened, becoming more exposed to solvent in the human crystal structure. Particularly, a salt bridge stabilized the human IL18 structure at the helix configuration, linking the helix to the core region. We observed that the bivalent binding mode for the human tetramer, which is disturbing one side of the tetramer by breaking the disulfide bonds, did not affect the stability of the complex, and thereby the tetramer remained intact. Hence, the tetramer formation of IL18-IL18BP can be beneficial to the host as it provides an additional stability advantage. Overall, our results show that the short IL18 epitope between the amino acids 68 and 81 mediates stability and self-assembly of IL18-IL18BP heterodimers.

Key words: Interleukin-18, Interleukin-18 binding protein, Protein-protein interactions, Self-assembly, Molecular dynamics simulation

ÖZET

IL18-IL18BP HETERODİMERLERİNİN DİNAMİKLERİNİ VE KENDİLİĞİNDEN MONTAJINI ANLAMAK İÇİN İNSAN IL18 YAPILARININ İNCELENMESİ

Yılmaz Yücehan Yazıcı
Moleküler Biyoloji ve Genetik Yüksek Lisans
Tez danışmanı: Serkan Belkaya
Eş danışman: Emel Timuçin
Ağustos 2023

Interleukin-18 (IL18), hem doğal hem de kazanılmış bağışıklığın düzenlenmesinde yer alan enflamatuar bir sitokindir. IL18 aktivitesi, sürekli olarak salgılanan IL18 inhibitörü IL18 bağlayıcı protein (IL18BP) tarafından sıkı bir şekilde düzenlenmektedir. İnsandan çiçek virüslerine kadar bilinen tüm IL18BP'ler aynı protein katlanmasını paylaşırlar. İnsan IL18'in bilinen kristal yapılarının araştırılması, IL18'in serbest veya sinyal komplekslerinde 3_{10} sarmal bir yapı benimserken, 68. ve 81. amino asitler arasındaki bölgenin tüm IL18-IL18BP komplekslerinde ya eksik ya da düzensiz bir yapıda olduğunu gösterdi. Bu bölgedeki C74 kalıntısının, insan IL18-IL18BP tetramerik düzeneğinde yeni bir moleküller arası disülfit bağı oluşturduğu bildirildi. Yine de bu küçük yüzey epitopunun IL18'in stabilitesi ve kendi kendine montajı üzerindeki etkisi belirsizdir. İlk olarak, IL18-IL18BP heterodimerlerinin bu küçük yüzey bölgesinin dinamiklerini moleküler dinamik simülasyonları ile araştırdık. Simülasyonlarda, küçük yüzey bölgelerinin farklı katlanmasını gözlemlemek için IL18-IL18BP'nin bilinen tüm kristal yapılarını ve AlphaFold2 ve homoloji modellemesi ile oluşturulan iki ek bilgisayar modelini kullandık. Daha sonra, önerdiğimiz insan ve Yaba benzeri hastalık virüsü

tetramerlerini oluşturduk ve bunları moleküller arası disülfit bağları olsun ya da olmasın analiz ettik. Küçük yüzeylerin sarmal yapısının esnekliği azaltarak kompleksin omurgasını stabilize ettiğini bulduk. Hesaplamalı modelimiz, serbest veya sinyal kompleksi üzerindeki IL18'e benzer şekilde daha kararlı ve daha az esnek bir kısa IL18 epitopuna katlanırken, insan veya virüs IL18BP'leri ile olan komplekslerdeki IL18, daha az kararlı bir omurgaya sahip esnek bölgeler gösterdi. İnsan kristalinin çekirdeği gevşedi ve insan kristal yapısında çözücüye daha fazla maruz kalacak hale geldi. Özellikle bir tuz köprüsü, sarmalı çekirdek bölgeye bağlayarak insan IL18 yapısını sarmal konfigürasyonda stabilize etti. Disülfit bağlarını kırarak tetramerin bir tarafını rahatsız eden insan tetramerinin bivalent bağlanma modunun kompleksin stabilitesini etkilemediğini ve dolayısıyla tetramerin sağlam kaldığını gözlemledik. Dolayısıyla, IL18-IL18BP'nin tetramer oluşumu, ek bir stabilite avantajı sağladığı için konağa faydalı olabilir. Genel olarak, sonuçlarımız, 68. ve 81. amino asitler arasındaki kısa IL18 epitopunun, IL18-IL18BP heterodimerlerinin stabilitesine ve kendi kendine montajına aracılık ettiğini göstermektedir.

Anahtar kelimeler: İnterlökin-18, İnterlökin-18 bağlayıcı proteini, Protein-protein ilişkisi, Kendiliğinden montaj, Moleküler dinamik simülasyonu

ACKNOWLEDGMENTS

First and foremost, I would like to express my gratitude to my advisor Dr. Serkan Belkaya, who opened the door of his lab and provided a new page for my life. I was fortunate to work under his supervision as he always remained diligent and passionate about his work. This motivated me to reach my excellence in the short time I spent here. He was always aware of my shortcomings and guided and supported me to push and improve my limits. It was a privilege to learn from him to be an excellent scientist, but moreover, I was able to learn more about life itself thanks to his thoughtful advice.

I would also like to express my gratitude to my co-advisor Dr. Emel Timuçin, for her support, trust, and patience. Thanks to her guidance, I was able to keep my head up and was able to overcome problems by thinking out of the box. Her insight and vast knowledge of the subject guided me through this research. I am extremely grateful for the opportunity to work with and learn from her.

I would like to express my appreciation to the esteemed committee members, Dr. Ilyas Chachoua and Dr. Perinur Bozaykut Eker, for their invaluable contributions and helpful feedback throughout this thesis.

I am thankful for all the former and current lab members, Güneş Tepe, Umut Tank, Ladin Işık Köse, Aysima Atılgan, Alperen Baran and Tunahan Çalıkoğlu. They were always helpful, supportive, and considerate.

TABLE OF CONTENTS

LIST OF TABLES

LIST OF FIGURES

ABBREVIATIONS

AF2	AlphaFold2
ASA	Accessible surface area
Cα	Alpha Carbon
CD	Cluster of differentiation
cos	Cosine
DAMP	Danger-associated molecular pattern
dPCA	Dihedral angle Principal Component Analysis
FEL	Free energy landscape
hIL18	Human Interleukin-18
hIL18BP	Human Interleukin-18 binding protein
IFN	Interferon
Ig	Immunoglobulin
IL	Interleukin
IL18BP	Interleukin-18 binding protein
IL18R	Interleukin-18 receptor
IRAK	Interleukin-1 receptor-associated kinase
kDA	Kilodalton
MD	Molecular dynamics
mRNA	Messenger Ribonucleic acid
MyD88	Myeloid differentiation factor 88
NK	Natural killer
PAE	Predicted aligned error
PAMP	Pathogen-associated molecular pattern
PC	Principal component
PCA	Principal component analysis
PDB	Protein Data Bank
plDDT	Predicted local distance difference test
pro-IL18	Precursor Interleukin-18
rASA	Relative accessible surface area
R_g	Radius of gyration
RMSD	Root mean square displacement
RMSF	Root mean square fluctuation
RNA	Ribonucleic acid
SASA	Solvent accessible surface area

sin	Sine
Th	T-helper
TIR	Toll-like/Interleukin-1 receptor
TNF	Tumor necrosis factor
vIL18BP	Viral Interleukin-18 binding protein
YLDV	Yaba-like disease virus

CHAPTER 1

Introduction

1.1 Interleukin-18

Interleukin (IL)-18 (IL18), known as a potent inducer of Interferon-γ (IFNγ), is a member of the IL1 family cytokines [1,2]. It is involved in the regulation of both adaptive and innate immunity in vertebrates [1–5]. Dysregulation of IL18 activity has been implicated in various immune-related diseases in humans [1,6–9].

1.1.1 Production of IL18

The location of *IL18* is on the human 11th chromosome. The gene consists of seven exons, of which exons 1 and 2 are non-coding and contain a GC-rich region and binding sites for the transcription factor, PU.1, specific to hematopoietic cells [10,11]. Both sites are considered to be required for basal *IL18* transcriptional activity. *IL18* mRNA expression is known to be induced upon various stimuli including pathogen-associated molecular patterns (PAMPs), danger-associated molecular patterns (DAMPs), and other inflammatory cytokines [1,5,8,12,13]. In comparison with other cytokines, IL18 exhibits more stability owing to the presence of fewer RNA-destabilizing elements in its mRNA [3,4]. Additionally, *IL18* expression is controlled post-transcriptionally by multiple microRNAs, such as microRNA-197 and microRNA-346 [9,14]. Similar to other IL1 family members, IL18 is initially produced as an inactive precursor of 193 amino acids (24 kDa) without a signal peptide [15]. Hence, this precursor form, pro-IL18, is localized

and accumulated mainly in the cytosol [15]. In response to inflammasome activation upon recognition of PAMPs or DAMPs, caspase-1 cleaves the inactive pro-IL18 at its N-terminus and promotes the release of the mature IL18 by initiating an inflammatory cell death program known as pyroptosis, which leads to the formation of pores in the cell membrane [4,9]. There have been also additional mechanisms independent of canonical caspase-1-mediated IL18 processing described [3,8,9,15]. Caspase-8 can induce activation and maturation of IL1β and IL18 in a Fas-dependent manner [3,16,17]. Additionally, proteases ,such as Proteinase 3, chymase, and granzyme B, are capable of extracellular processing pro-IL18 released from dying cells without the involvement of an inflammasome [3,18–20]. *IL18* mRNA is constitutively expressed at varying levels by many cell types, such as Kupffer cells, macrophages, dendritic cells, hepatocytes, keratinocytes, astrocytes, microglia, and osteoblasts [1,2,4,9,21–24] However, mature IL18 is secreted predominantly by myeloid cells, such as macrophages and dendritic cells [1,25,26].

1.1.2 IL18 signaling

The IL18 signaling complex assembles by combination of IL18, a ligand-binding chain known as IL18Rα, and a signal-transducing chain known as IL18Rβ [8,27,28]. While IL18Rα is constitutively expressed at low levels in various cell types [1,29]. IL18Rβ expression is more restricted, found only in a small population of immune cells, such as T cells, Natural killer (NK) cells, and NKT cells [1,29]. IL12 and IFNα are known to induce the expression of IL18R in human NK and T cells [9,30,31]. IL18Rβ is not able to form any heterodimer with either IL18 or IL18Rα and therefore binds to the IL18-IL18Rα heterodimer assembly to form IL18 ternary signaling complex [15,32,33]. Both

IL18Rα and IL18Rβ belong to the IL1 receptor family and contain a Toll-like/IL1 receptor (TIR) domain on their cytoplasmic side similar to the Toll-like receptors (TLRs) [3,10]. TIR domains on the IL18-IL18R complex relay the signal into Myeloid differentiation factor 88 (MyD88) and form a TIR-TIR interface [4,34]. The MyD88 complex initiates the formation of the Myddosome signaling complex by recruiting the Interleukin-1 receptor-associated kinase 1 (IRAK1), IRAK2, and IRAK4 [3,9,15,35]. Phosphorylated IRAK4 binds to tumor necrosis factor (TNF) receptor-associated factor 6 (TRAF6), which in turn activates the inhibitor of κB (IκB) kinase (IKK) [12,15,28]. Following ubiquitination of the IκB upon phosphorylation by IKK, the nuclear factor kappa-light-chain-enhancer of activated B cells (NF-κB) became liberated and translocated to the nucleus, resulting in transcription of inflammatory genes [3,4,9,15,28,36] (Figure 1.1). IL18 signaling has also been shown to activate mitogen-activated protein kinase (MAPK), Signal transducer and activator of transcription 3 (STAT3) and c-Jun N-terminal kinase (JNK) pathways [12,15,28,35,37–39]. Overall, IL18-mediated signaling culminates in induction of various inflammatory mediators implicated in modulating both innate and adaptive immune responses.

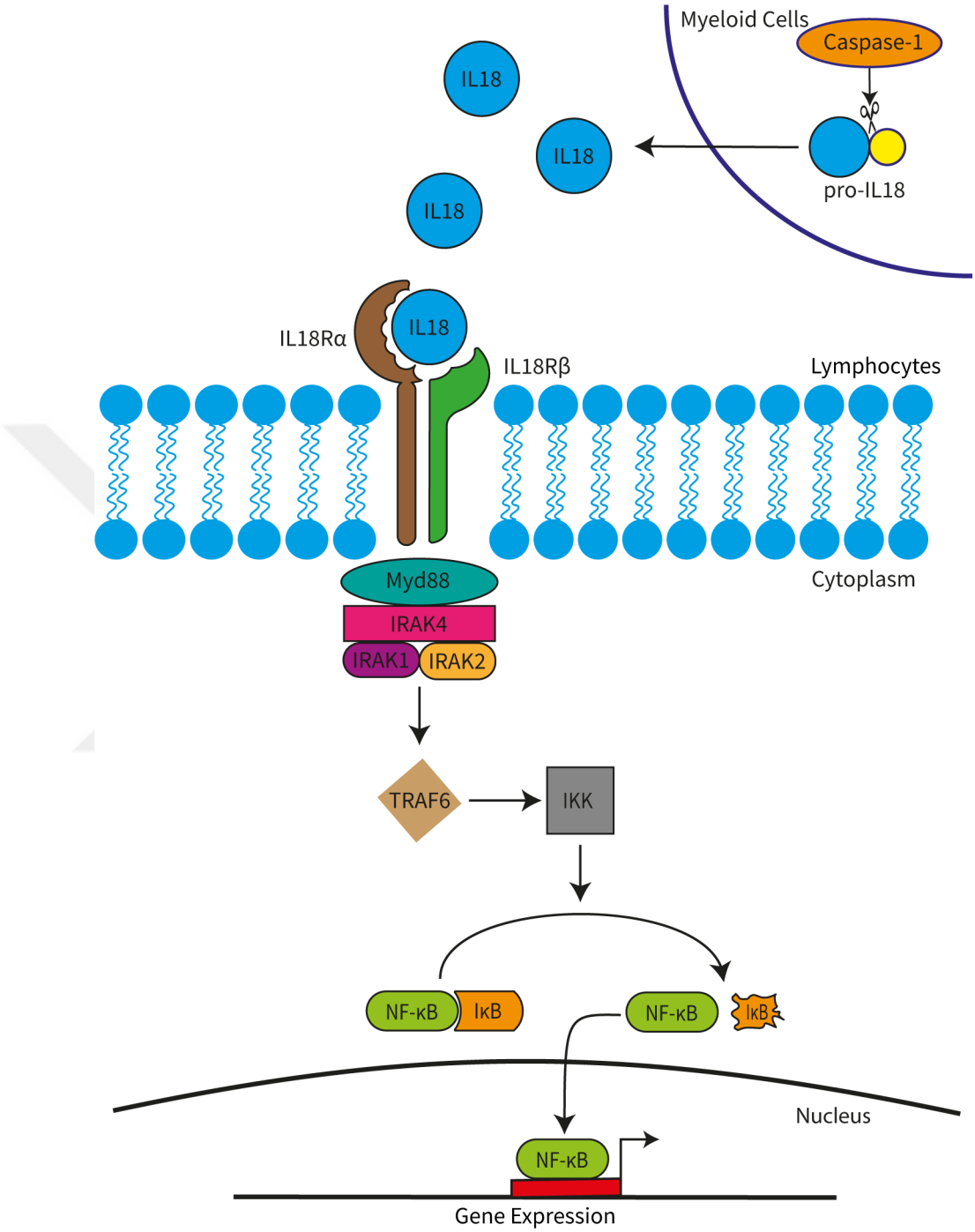

Figure 1.1 IL18 signaling. (Redrawn from Hirooka Y et al., 2019 [28])

1.1.3 Role of IL18 in immune system

IL18 is a pleiotropic inflammatory cytokine, characterized by its ability to stimulate multiple cell types, but many of its biological functions are exerted in synergism with other cytokines. IL18, in combination with IL12 or IL15, primarily activates $CD4^+$ T helper 1 (Th1) cells, $CD8^+$ T cells, and NK cells, inducing production of IFNγ, which is essential for host defense against intracellular pathogens and tumors [3,5,9,40]. IL18 stimulation together with IL12 and IL15 has been shown to induce generation of memory-like NK cells against cancer cells [3,41–43]. IL18 in combination with IL12 can also activate macrophages [9,44,45]. Moreover, IL12 and IL18 together induce IgG2a production in B cells while suppressing IL4-dependent IgE and IgG1 expression [9,46,47]. IL18 without IL12 or IL15 does not induce IFNγ, but IL4 and IL13 in T cells, thus promoting a Th2 response, which is responsible for allergic reactions and killing extracellular parasites and bacterial infections [9,15,48]. Lastly, IL18 can also induce production of many other mediators, such as nitric oxide, TNFα, Fas ligand, IL6, and IL8, involved in inflammation, cell survival and differentiation [1,9,25,49–51]. Overall, pleiotropic characteristics of IL18 imply that its activity must be tightly regulated in order to preserve host homeostasis and prevent hyper-inflammation.

1.1.4 Regulation of IL18 activity

IL18 expression is regulated at both mRNA and protein levels. Mature IL18 activity is directly regulated by its natural antagonist, IL18 binding protein (IL18BP). IL18BP blocks the binding between the IL18 and IL18Rα [1,8,52]. It is a free soluble protein with a higher binding affinity to IL18 compared to that of IL18 to IL18Rα, preventing the IL18 signaling complex formation by blocking the interface between IL18 and IL18Rα

[1,52,53]. IL37, an IL1 family member, is another inhibitor of IL18 signaling by forming a complex of IL37, IL18Rα and IL1R8, which cannot bind to MyD88 but induces an anti-inflammatory signal to the cell [54,55].

1.2 IL18BP

IL18BP, like *IL18*, is found in chromosome 11 in the human genome. *IL18BP* mRNA undergoes alternative splicing, leading to generation of four known protein isoforms of IL18BP: a, b, c, and d. IL18BPa and IL18BPc isoforms contain an immunoglobulin (Ig) domain for IL18 binding, whereas IL18BPb and IL18BPd isoforms do not have a complete Ig domain, thereby lacking IL18 binding and inhibitory activity [4,56]. Human IL18BPa is the canonical isoform, whereas physiological abundance of other isoforms is dubious [4,6,56]. Therefore, IL18BPa will be termed and hereafter used as IL18BP in the text throughout the thesis. IL18BP is constitutively secreted and its basal circulating levels in humans are very low, ranging between 2 and 10 ng/mL [4,6,12,57,58]. IL18BP is expressed by various cell types including both hematopoietic and non-hematopoietic cells [1,8,12,59]. IFNγ is known to be potent inducer of IL18BP expression, generating a negative feedback mechanism for down-regulation of IL18 activity (Figure 1.2) [12,60–62]. In addition, TNFα, IFNβ, and IL27 were also shown to induce IL18BP albeit to a dramatically lower extent compared to IFNγ [5,12,63–65].

The imbalance between IL18 and IL18BP has been implicated in infection, cancer, and many inflammatory diseases affecting various systems including adult-onset Still's disease, systemic juvenile idiopathic arthritis, inflammatory bowel diseases, myasthenia gravis, pyogenic arthritis, pyoderma gangrenosum and acne, type 1 diabetes, multiple sclerosis, systemic lupus erythematosus, hepatitis, polymyositis and dermatomyositis

[1,8,12,52,66–70]. In particular, high levels of IL18 activity have been reported in macrophage activation syndrome and hemophagocytic lymphohistiocytosis, which are typically life-threatening complications of rheumatological diseases and infections, respectively [12,66,71,72]. Recently, inherited human IL18BP deficiency was described in a child with fulminant hepatitis upon infection with Hepatitis A virus [6]. Uncontrolled IL18 activity was implicated in absence of IL18BP, resulting in excessive activation of lymphocytes and macrophages in the infected liver, thereby massive hepatocyte death and liver failure [6]. In the end, better understanding of the interactions between IL18, IL18BP and IL18R is a necessity for the development of novel and/or better remedies for such pathological conditions related to dysregulation of IL18 activity.

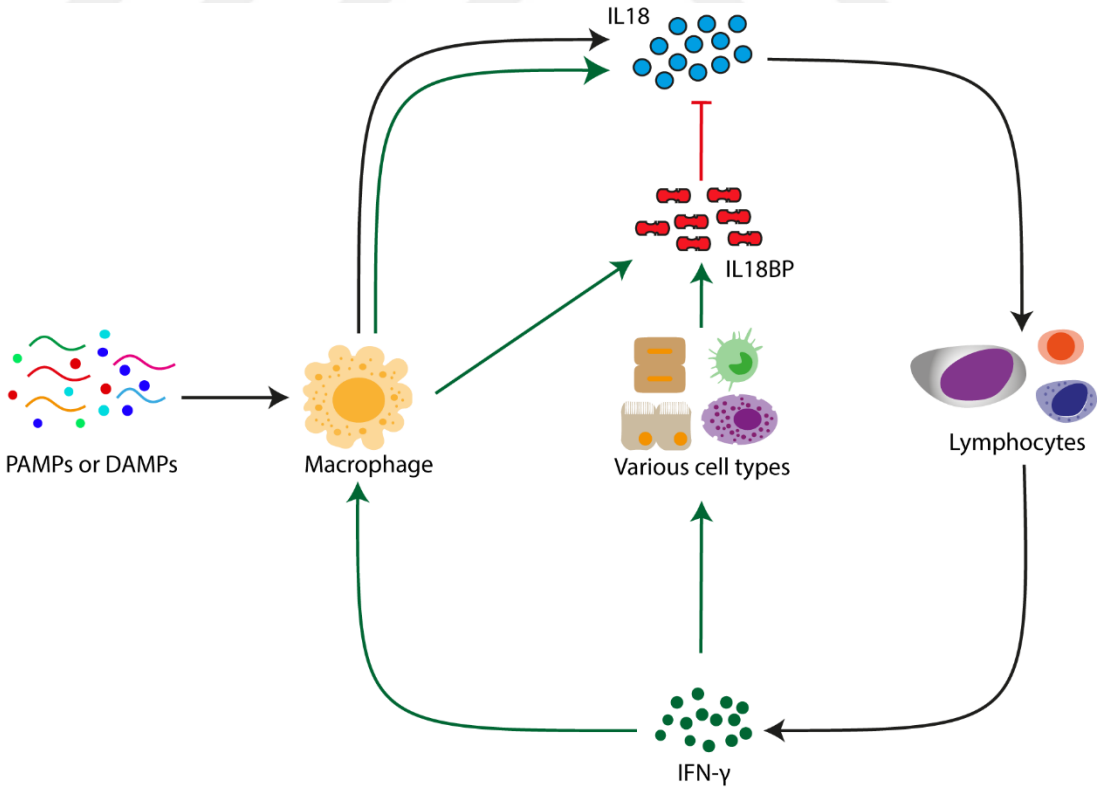

Figure 1.2 IL18 is regulated by IL18BP. (Redrawn from Belkaya S et al., 2019 [6])

1.3 Interaction between IL18 and IL18BP

The quaternary structure of IL18 folds into a β-trefoil fold with 12 β-strands, one short α-helix, and one 3_{10}-helix [33,73]. It has been noted that binding of the IL18Rα did not affect the structure of IL18 in their crystal structure as all β-strands, short α-helix, and one 3_{10}-helix preserved their configuration [33,53,74]. The IL18BP inhibits the binding of IL18 and IL18Rα by blocking the interference between IL18 and IL18Rα-D3 site (Figure 1.3) [53].

Many poxviruses, such as Molluscum contagiosum virus, orthopoxviruses such as Variola virus, and yatapoxviruses, such as Yaba-like disease virus (YLDV), use an IL18 decoy protein, viral IL18BP (vIL18BP), to suppress the host immune responses [73,75]. The crystal structure of this vIL18BP shows high structural similarity with human IL18BP (hIL18BP) [76]. Hence, IL18 inhibitory mechanism of IL18BP is conserved among other species, and based on the competition for the interaction interface of IL18 and IL18Rα [73,75,76]. In addition to the conserved binding mechanism between human and viral IL18BPs despite their low sequence similarities, IL18 and IL18BP share the same binding interface and occupy the same surface surrounding the similar residues as the mutation of K53 residue on human IL18 (hIL18) reduces the binding affinity of both human and viral IL18BPs [73,75,77,78].

The binding of the hIL18 to hIL18BP shows a rigid binding model as both structures remain in their similar configuration [76]. Additionally, the binding of IL18 to IL18Rα, IL18Rβ, or antibody against IL18 does not drive into new conformation on the surface of IL18 [53,74]. Although IL18-IL18BP displays a rigid binding mechanism, and the overall structure of bound and free state stays relatively the same, the distant surface region of IL18 corresponding to a short stretch of amino acids between 68 and 81 shows

a disordered conformation in the IL18-IL18BP complexes (Figure 1.3) [73,75,76]. In all the different sources of IL18 and IL18BP crystal structures, distant surface regions display higher flexibility or lack secondary structure [73,75,76], whereas the conformation of the small surface region folds to compact 3_{10} helical forms for IL18 in the IL18-IL18R complex or free form of IL18 (Figure 1.3). Despite that human and viral IL18BPs show a similar inhibition pattern and use the same binding surface on the IL18, they demonstrate different quaternary structures. For example, tetra-partite assembly is observed for the human IL18 complex with the YLDV IL18BP (Protein Data Bank (PDB) ID: 4eee) while complex between ectromelia virus IL18BP and hIL18 shows heterodimer (PDB ID: 3f62) [73,75]. The recent study that revealed the crystal structures of human IL18-IL18BP also indicated the possibility of the tetramer complex [76]. A possible novel symmetry-related tetrameric assembly has been proposed by using the intermolecular disulfide contacts between IL18 and IL18BP [76]. The C74 on the IL18 is found within the flexible distant surface region and reported to form a novel intermolecular disulfide bridge with IL18BP [76]. The new finding suggests that IL18-IL18BP complexes show high elasticity as can be found in quaternary structures mediated by disulfide contacts.

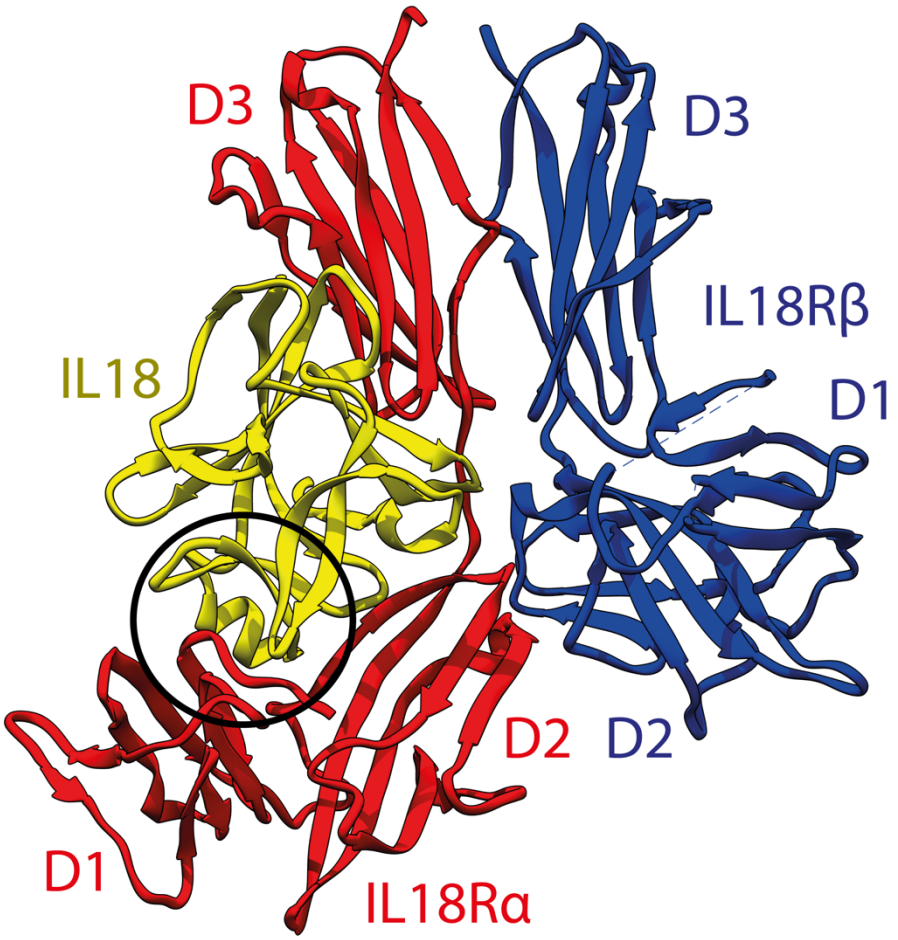

Figure 1.3 Schematic representation of crystal structure (PDB: 3wo4) of human IL18-IL18R complex. Domains (D1-D3) are shown on IL18Rα (red) and IL18Rβ (blue). The small surface epitope between the 67th and 81st residues on IL18 (yellow) is indicated by black circle. (Adapted from Tsutsumi N et al., 2014 [53])

1.4 Aim of the study

The viral and host crystal structures of IL18-IL18BP complexes provided essential information regarding the mechanisms of IL18 inhibition by IL18BPs. However, the static models obtained from the crystal structures do not provide necessary information on how conformational dynamics is affected during the assembly of IL18-IL18BP

complexes. Additionally, how short surface epitope affects the stability of the heterodimer or self-assembly of IL18-IL18BP complexes remains vague. Molecular dynamics (MD) simulation is a useful computational method for analyzing the conformational dynamics of proteins, using the atomic level information of biomolecules to arrange computational space. MD simulations of the IL18-IL18BP complexes may address the importance of the epitope between the residues 68 and 81 on IL18.

The work presented in this thesis was originally published as "Yazıcı, Y.Y., Belkaya, S., & Timucin, E. A small non-interface surface epitope in human IL18 mediates the dynamics and self-assembly of IL18-IL18BP heterodimers. Computational and Structural Biotechnology Journal. (2023, July 1) 21:3522-3531. eCollection 2023. https://doi.org/10.1016/j.csbj.2023.06.021"

CHAPTER 2

Methods

2.1 Homology modeling of the core region of human IL18BP

The human IL18BP (UniProt ID: O95998) was predicted by MODELLER v9.25 containing residues from 20 to 170, employing the YLDV IL18BP structure (PDB ID: 4ekx) as the template [79]. A discrete optimized protein energy score was used to determine the best possible structure that represents the IL18BP [80]. The final structures were evaluated and selected to be free from Ramachandran outliers.

2.2 Docking-based prediction of the human IL18-IL18BP complex

The IL18 structures were obtained from different PDB structures of IL18-IL18R complex (PDB IDs: 3wo2, 3wo3, 3wo4, and 4r6u) [53,74]. The missing region within the IL18 in the structure was predicted by MODELLER [79]. First, rigid docking using ClusPro algorithm was performed to generate human IL18-IL18BP models based on IL18 structures from different PDB sources and computationally generated hIL18BP structure[81]. Top-scoring ClusPro predictions were superimposed to identify the predominant binding interface and the amino acids lining this interface. Next, HADDOCK calculations were performed by using the selected complex from ClusPro and preserving the flexible loop interface [82]. The final structures of IL18-IL18BP were selected based on the docking score from the top structure of each HADDOCK cluster. Overall, each run consisted of 4 different hIL18 and homology model of hIL18BP.

2.3 AlphaFold2 prediction of the human IL18-IL18BP complex

We utilized AlphaFold2 (AF2) to predict human IL18BP in both the free form and the IL18-IL18BP complex forms [83–85]. MMseqs2 was employed to generate multiple sequence alignments using the databases of UniRef100 [86–88] and PDB70 (version 05Sep15), which is a clustered version of PDB [89]. The final model was relaxed by the AMBER force field [90]. The top-ranked structure was selected and analyzed based on residue confidence scores and predicted aligned error (PAE) plots.

2.4 MD simulations

Five human IL18-IL18BP heterodimers were analyzed by the MD simulation. The first three heterodimers were directly extracted from PDB (PDB IDs: 7al7, 3f62, 4ekx), and the remaining two were generated by homology modeling and AF2-based predictions. The viral tetramer from YLDV (4eee) and the symmetry-related human tetramer were modeled with (S-S) or without (-SH) the intermolecular disulfide bonds. The PDB structure were refined with MODELLER by modeling absent non-terminal regions and removing all of the nonstandard residues in the PDB structures [79]. Overall, nine different IL18-IL18BP complexes were placed in the center of a cubic water box with a padding distance of 10 Å and neutralized to a final concentration of 0.15 M using Na^+ and Cl^- counter ions. Systems were simulated by the GROMACS algorithm with the CHARMM36 force field containing the correction map [91–95]. The TIP3P model was implemented for water [96]. For all simulations, periodic boundary conditions and a time-step of 2 fs were applied. Long-range electrostatic interactions were computed by the Particle-mesh Ewald summation method with a grid spacing of 1.2 Å and a cut-off value of 12 Å was used for short-range interactions [97]. Resulting MD systems were first

minimized with 40,000 steps by the steepest descent method and then equilibrated using a constant-volume ensemble (NVT) with Berendsen thermostat and an isothermal-isobaric ensemble (NPT) with Parinello-Rahman pressure coupling at 1 atm and 310 K. Lastly, production simulations were performed for 500 ns. Details of the MD systems were given in Table 2.1.

Table 2. 1 Details of MD systems.

System	IL18 Source	IL18BP Source	Stoichiometry	MD (ns)
4eee (S-S)	YLDV	YLDV	2:2	500
4eee (-SH)	YLDV	YLDV	2:2	311
7al7 (S-S)	Human	Human	2:2	100
7al7 (-SH)	Human	Human	2:2	500
4ekx	YLDV	YLDV	1:1	500
3f62	Ectromelia virus	Ectromelia virus	1:1	500
7al7	Human	Human	1:1	500
7al7	Human	Human	1:1	396
AF2	Human (comp)	Human (comp)	1:1	500
Model	Human (comp)	Human (comp)	1:1	500

Human IL18 was used for all systems.
Tetramers were simulated in the presence (S-S) and absence of (-SH) of the intermolecular disulfide bond(s). comp: Computational model.

(Adapted from Yazıcı YY et al., 2023 [98])

2.5 Data analysis

Root mean square displacement (RMSD) and root mean square fluctuation (RMSF) of Cα atoms, the radius of gyration (R_g), and solvent accessible surface area (SASA) were calculated for each complex and their subunits. Trajectories were visualized by utilizing Visual Molecular Dynamics [99]. All-to-all RMSD heatmaps were calculated by MDAnalysis [100]. Bio3D was used to describe the dynamics of each complex by calculating and analyzing principal component analysis (PCA) [101]. Covariance matrix

of Cij was obtained by using mass-weighted Cartesian coordinates of the Cα atoms as follows:

$$C_{ij} = \langle (q_i - \langle q_i \rangle)(q_j - \langle q_j \rangle) \rangle$$

wherein q_i and q_j correspond to the internal coordinates of atoms *i* and *j*, respectively; $\langle ... \rangle$ defines the ensemble average. Next, principal components (PCs) are calculated by eigendecomposition on the C_{ij}. A two-dimensional free energy landscape (FEL) was also constructed using the first two PCs as follows:

$$\Delta G(x) = -k_b T ln P \left(\frac{P(V_{\max})}{P_{max}(V)} \right)$$

wherein k_B is the Boltzmann constant, and T is the absolute temperature. $P(V_x)$ and $P_{max}(V)$ are probabilities from the MD data, with $P_{max}(V)$ representing the most probable state.

Dihedral angle principal component analysis (dPCA) method, which uses dihedral angles of the protein backbone, was also carried out. For some structures, dPCA has been shown to produce better description of the conformation space than cartesian PCA [102,103]. Because dihedral angles are periodic non-linear values as opposed to Euclidean distance, sin (sine) and cos (cosine) transformations of dihedral angle was applied to transform the angular periodic behavior to linear coordinate space. To this end, dPCA formula is extended as:

$$q_{2n-1} = cos\Psi_n \qquad q_{2n} = sin\Psi_n$$

where n is the total number of peptide backbone and side chain, ψ is the dihedral angles. Both ψ and ϕ can be used to generate the covariate matrix. Employing the Gibbs energy formulation gives the dPCA FEL.

CHAPTER 3

Results

The work presented in this thesis was originally published as "Yazıcı, Y.Y., Belkaya, S., & Timucin, E. A small non-interface surface epitope in human IL18 mediates the dynamics and self-assembly of IL18-IL18BP heterodimers. Computational and Structural Biotechnology Journal. (2023, July 1) 21:3522-3531. eCollection 2023. https://doi.org/10.1016/j.csbj.2023.06.021"

3.1 Computational prediction of the structure of human IL18-IL18BP complex

Human computational model of the IL18-IL18BP complex was generated using homology modeling and AF2. The structure obtained from the AF2 prediction gave high confidence score and low residual position error for the IL18-IL18BP complex (Figure 3.1a). There were no positional error or low confidence regions in the interface between the IL18 and IL18BP. The RMSD calculation based on the Cα- and all-atom of the computational model against the reference crystal structure (7al7) scored below 2 Å for the total or any subunits of the complex molecule (Figure 3.1b and Table 3.1). Both AF2 and homology models were generated before the registry of the human crystal structure of the IL18-IL18BP complex to the database. Hence, the highly accurate computational model of IL18-IL18BP was generated without relying upon the crystal structure.

Table 3.1 Comparison of the computed models against the experimental structure.

	IL18		IL18BP	
	Cα	**all atom**	**Cα**	**all atom**
AF2	1.184	2.017	1.482	1.935
HM-Dock	1.815**	2.708**	1.078	1.799

Reference structure: 7al7. HM-Dock: Homology docking
**IL18 was obtained from the 3wo2 for the docking study.
(Adapted from Yazıcı YY et al., 2023 [98])

To obtain the homology predicted human IL18-IL18BP, the different sources of IL18 crystal structures were used, as given in the table (Table 3.2). Because different IL18 crystal structures showed variations, such as mutations and unfolded parts, the homology modeled hIL18BP were docked with human IL18s from different PDBs. The models produced by ClusPro rigid docking algorithm are superimposed onto the 7al7 crystal structure (Figure 3.2). The models showed the same docking interface between IL18-IL18BP picked for the HADDOCK flexible docking. The passive residues found in the interface for each model were defined with PRODIGY [104,105]. The best model of the IL18-IL18BP was selected from the HADDOCK model for the MD simulation. The results were first assessed by HADDOCK criteria based on clusters with the less HADDOCK score, interface RMSD, desolvation, Van der Waals energy, and higher fraction of common contact [104,106]. The final models were refined with water in the HADDOCK server and compared with each other (Figure 3.3). The homology model of IL18-IL18BP was selected using the 3wo2 as the IL18 structure source. The accuracy of a homology model of the human IL18-IL18BP complex using the 3wo2 was also comparable to the AF2 model (Figure 3.1b and Table 3.1).

Table 3.2 The IL18 crystal structures used in the docking study.

PDB Entry	Method	Resolution	Chain
3wo2	X-ray	2.33 Å	A
3wo3	X-ray	3.10 Å	C
3wo4	X-ray	3.10 Å	A
4eee	X-ray	2.71 Å	B
4ekx	X-ray	1.75 Å	D
4hjj	X-ray	2.10 Å	A
4r6u	X-ray	2.80 Å	B
4xfs	X-ray	1.91 Å	A
4xft	X-ray	2.00 Å	A
4xfu	X-ray	2.85 Å	A

Superimposing the homology model onto the reference structure displayed variations between each protein structure. The RMSD calculation of Cα and all-atom for the homology model against the crystal model scored a range between 1.8 to 2.7 Å considering both subunits (Table 3.1). The RMSD score of the homology model showed that the residues are positioned close with minimal error margin, which shows the accuracy of the IL18-IL18BP complex (Table 3.1). The comparison of both computational models is done by superimposing and calculating the Cα-RMSD of each subunit. The RMSD was calculated at 1.1 Å and 1 Å for IL18 and IL18BP, respectively, for the computational model.

Computational and experimental structures showed different secondary structures for the region of hIL18 encompassing the amino acids between 68 and 81. Computational models fold into 3_{10} helices for the small surface epitope similar to the experimental structure of IL18 in the free or receptor complex model (Figure 3.1c). Conversely, IL18 from the IL18-hIL18BP complex or IL18-vIL18BP adopted a disordered secondary

structure (Figure 3.1c). The C74 residue, which is located in this small surface region, is suggested to be important in the assembly of the tetramer [76]. Hence, in the study, both AF2 and homology-modeled IL18-IL18BP complexes were used to investigate the configuration of IL18's small region epitope and tetramer assembly (Figure 3.1c).

Different oligomeric conditions of the IL18-IL18BP tetramer complexes were assessed. The only available experimental tetramer structure is the YLDV IL18- IL18BP complex (PDB ID: 4eee) (Figure 3.4b), which is used in further steps. The human tetramer IL18-IL18BP complex was generated by positioning the human crystal of the IL18-IL18BP complex symmetrically and forming a disulfide bond between the C74 of IL18 and the C131 of hIL18BP (Figure 3.4c). The disulfide bond between the IL18 and IL18BP was either added or ignored for the tetramer assembly in order to compare the importance of the disulfide bond in the overall stability of the assembly. Overall, nine systems that have (i) different IL18BPs originating from different sources, human or virus, (ii) variable secondary structure of small surface region on IL18 and (iii) different assemblies were analyzed by MD simulations.

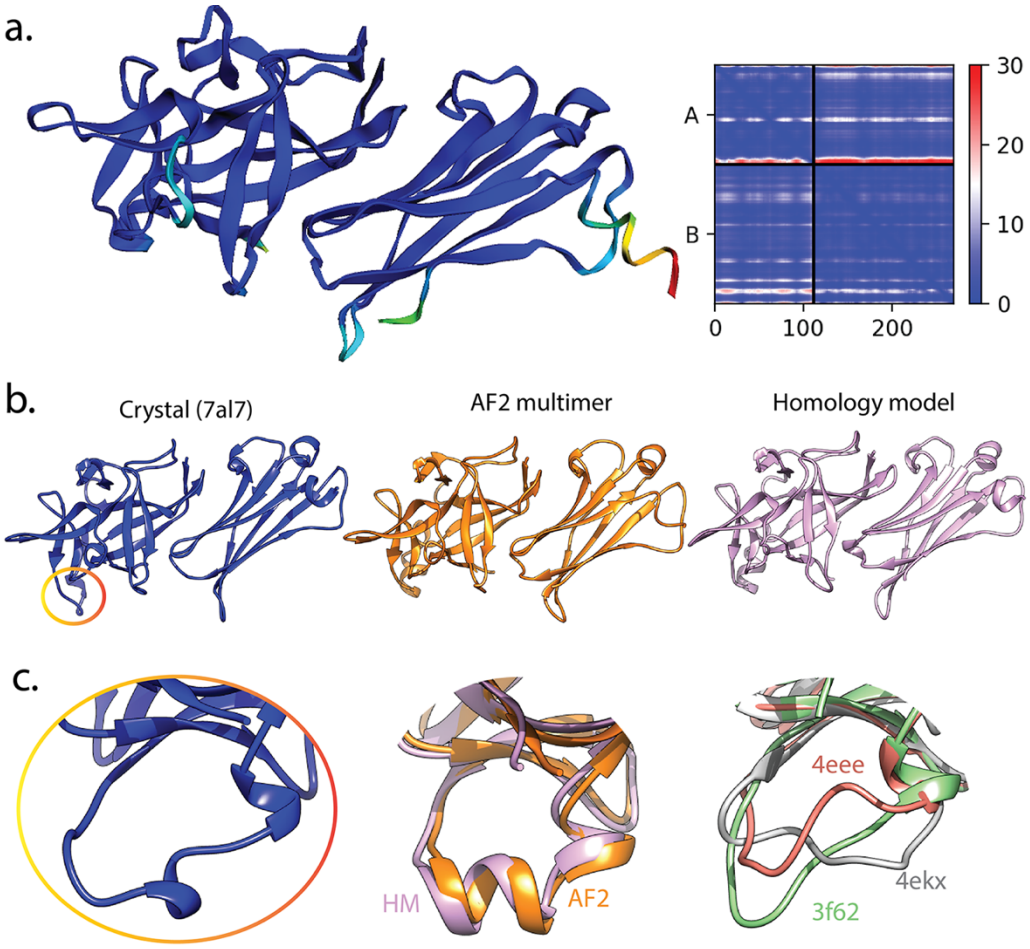

Figure 3.1 The experimental and predicted IL18-IL18BP complexes. (a) Panel shows the computed complex structure of human IL18-IL18BP by AF2, with coloring based on residue confidence score (plDDT: predicted local distance difference test, red: plDDT<50, yellow: plDDT<60, green: plDDT<70, cyan: plDDT<80, blue: plDDT<90). A PAE plot is also shown. Chain A shows IL18BP, and Chain B shows IL18. (b) Panel shows the superimposed structures of human crystal complex, AF2 multimer, and docking-based predictions. RMSD values for this comparison are given in Table 3.1. (c) Panel shows the small region with different conformations in the complexes analyzed in this study. (Adapted from Yazıcı YY et al., 2023 [98])

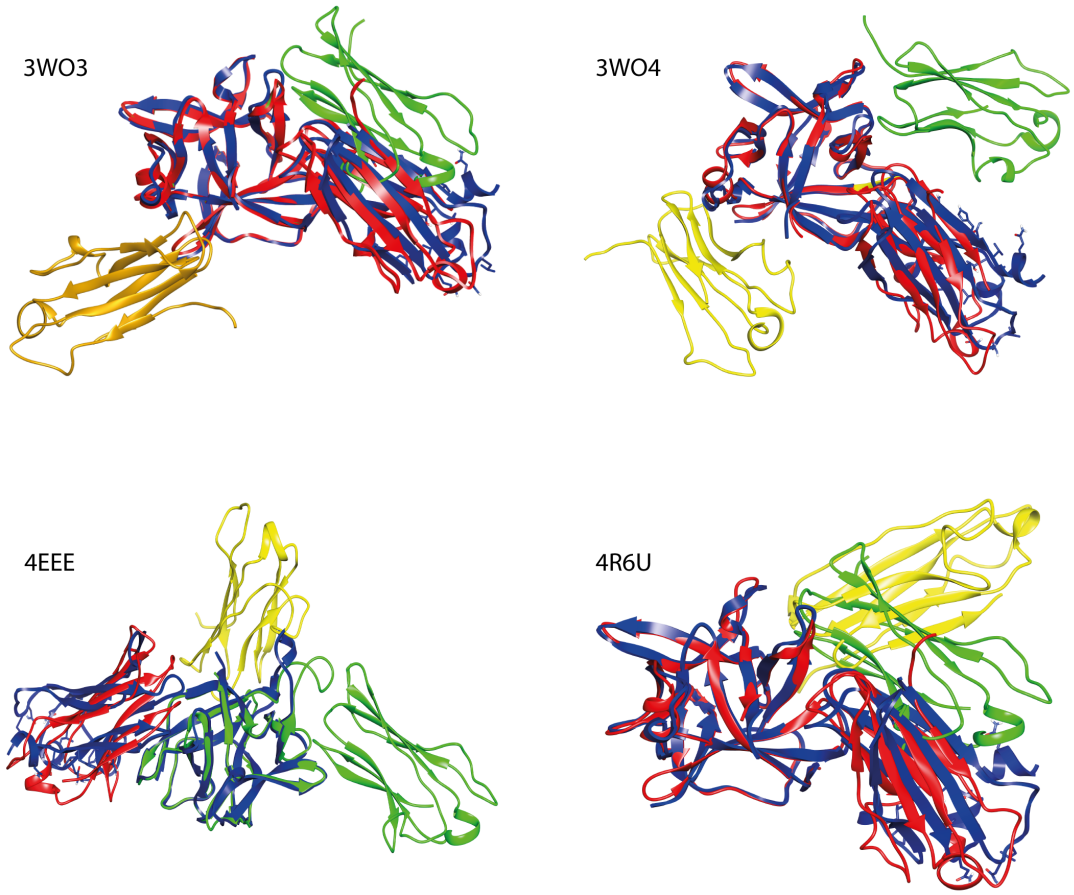

Figure 3.2 Docking of human IL18-IL18BP structures obtained from ClusPro. The figure shows the different IL18 structures used in the study as the source. ClusPro produces 10 different docking models based on its algorithm. The 3 docking models out of 10 is given for each IL18-IL18BP docking. The blue color indicates the 7al7 crystal structure. The red complex shows the highest similarity to the original crystal model. Green- and yellow-colored structures show alternative docking patterns produced by ClusPro.

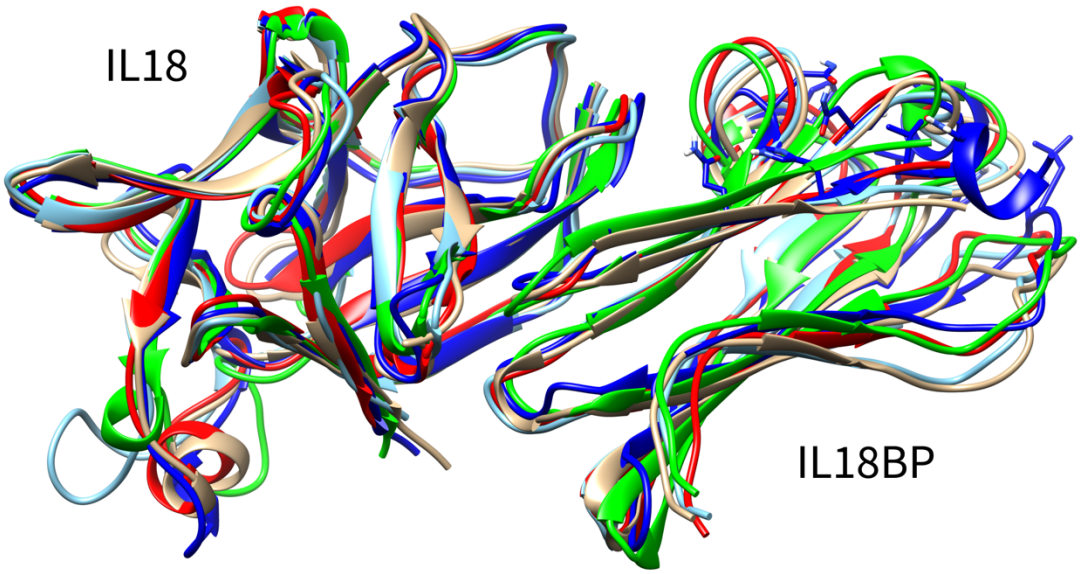

Figure 3.3 Docking of human IL18-IL18BP structures obtained from HADDOCK. The figure shows the models obtained upon refining within the HADDOCK server. The blue color depicts the 7al7 crystal structure. The red-, green-, teal-, and brown-colored structures illustrate the complex obtained by using the structure sources of IL18: 3wo4, 4eee, 4ekx, and 4r6u, respectively.

3.2. Origins of the IL18 and IL18BP affect the backbone mobility and shape of the complexes

The most flexible and highest backbone mobility was observed in the human crystal IL18-IL18BP complex (7al7) after calculating the all-to-all RMSD of each subunit in the complex (Figure 3.4). The change on the backbone of the human IL18-IL18BP complex was calculated as an average of 8 Å for Cα-RMSD. The virus model retrieved from the ectromelia virus (3f62) showed similar higher backbone mobility (Figure 3.4). The remaining heterodimers showed little variety and remained stable through simulation based on RMSD results. The tetramer molecules of 4eee and 7al7 showed different results for all RMSD. 4eee tetramer showed less mobility without a disulfide

bridge (Figure 3.4). Conversely, 7al7 without the disulfide bridge showed higher fluctuation, but the disulfide bridge stabilized the molecule and lowered backbone fluctuations (Figure 3.4).

R_g and SASA calculations were applied for the whole complex and each subunit to assess the change in the overall stability and the surface (Figure 3.5). Explicitly, the R_g and SASA values of the hIL18 ranged between 15-16 Å and 80-90 nm^2, respectively, while slightly wider ranges of 14-16 Å and 60-80 nm^2 were sampled for the decoy structures (Figure 3.5). Overall, these results show that different structures were obtained because of the different sources that IL18 and IL18BP were retrieved from.

Compared to other experimental models, IL18BP retrieved from the ectromelia virus showed a more packed configuration, and the average R_g was calculated as 20.5 Å for the given model (Figure 3.5a, green line). Nevertheless, SASA calculation for all IL18-IL18BP complexes remained relatively similar, while the ectromelia virus model scored an average of 150 nm^2 for SASA calculation (Figure 3.5b). The difference between R_g and SASA might arise from the fact that the monomer or heterodimer calculation of the protein might not appear globular in shape (Figure 3.5). This phenomenon gives an advantage to SASA calculation and provides a better understanding of the overall shape of the molecule rather than relying only on the R_g values [107]. Although many complexes remained stable, the human IL18-IL18BP complex obtained from crystal structure showed the greatest variation in the R_g and SASA measurement (Figure 3.5). If the results from the all-RMSD were considered, the human crystal model begins to loosen throughout the simulation, which is indicated by the upward increase in both R_g and SASA calculations (Figures 3.4 and 3.5). The computational models remained stable,

and no sudden changes occurred in their R_g or SASA measurement, indicating that the small surface region on hIL18 influences the dynamics of the backbone of the complex.

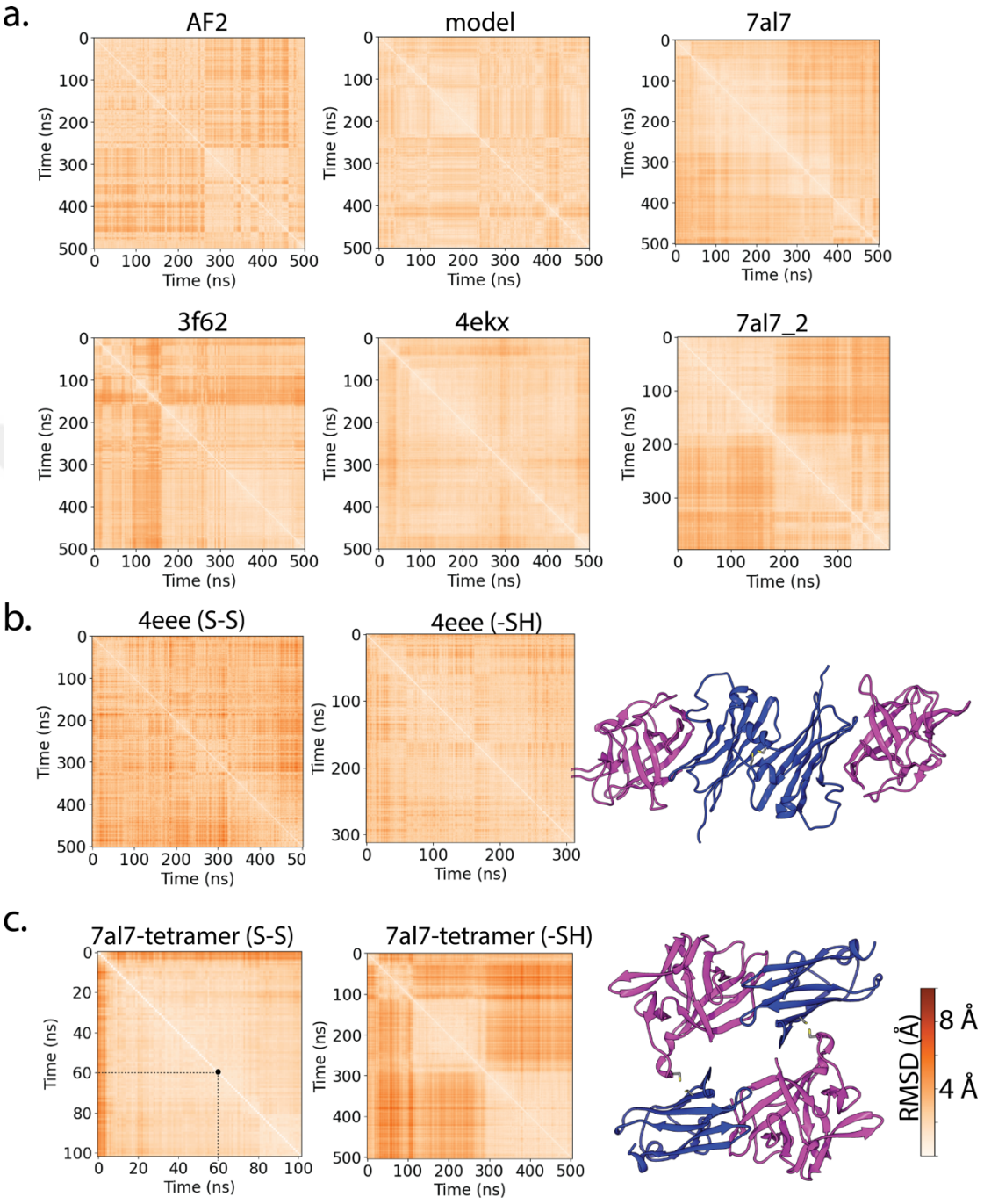

Figure 3.4 All RMSD plots of the human IL18-IL18BP models used in the study. All-to-all RMSD plots based on Ca traces. (a) Panel shows the human IL18-IL18BP dimers obtained from AlphaFold2, homology modeling and docking, and the recent crystallization study. (b) Panel shows the hIL18 crystal complexes formed with viral IL18BPs. (c) Panel shows the tetrameric assembly of the 4eee complex. Blue shades RMSD heatmaps show each IL18-IL18BP dimer in the tetramer. (The tetramers with and without the intermolecular bond(s) were labeled; oxidized form: S-S, reduced form: -SH). (Adapted from Yazıcı YY et al., 2023 [98])

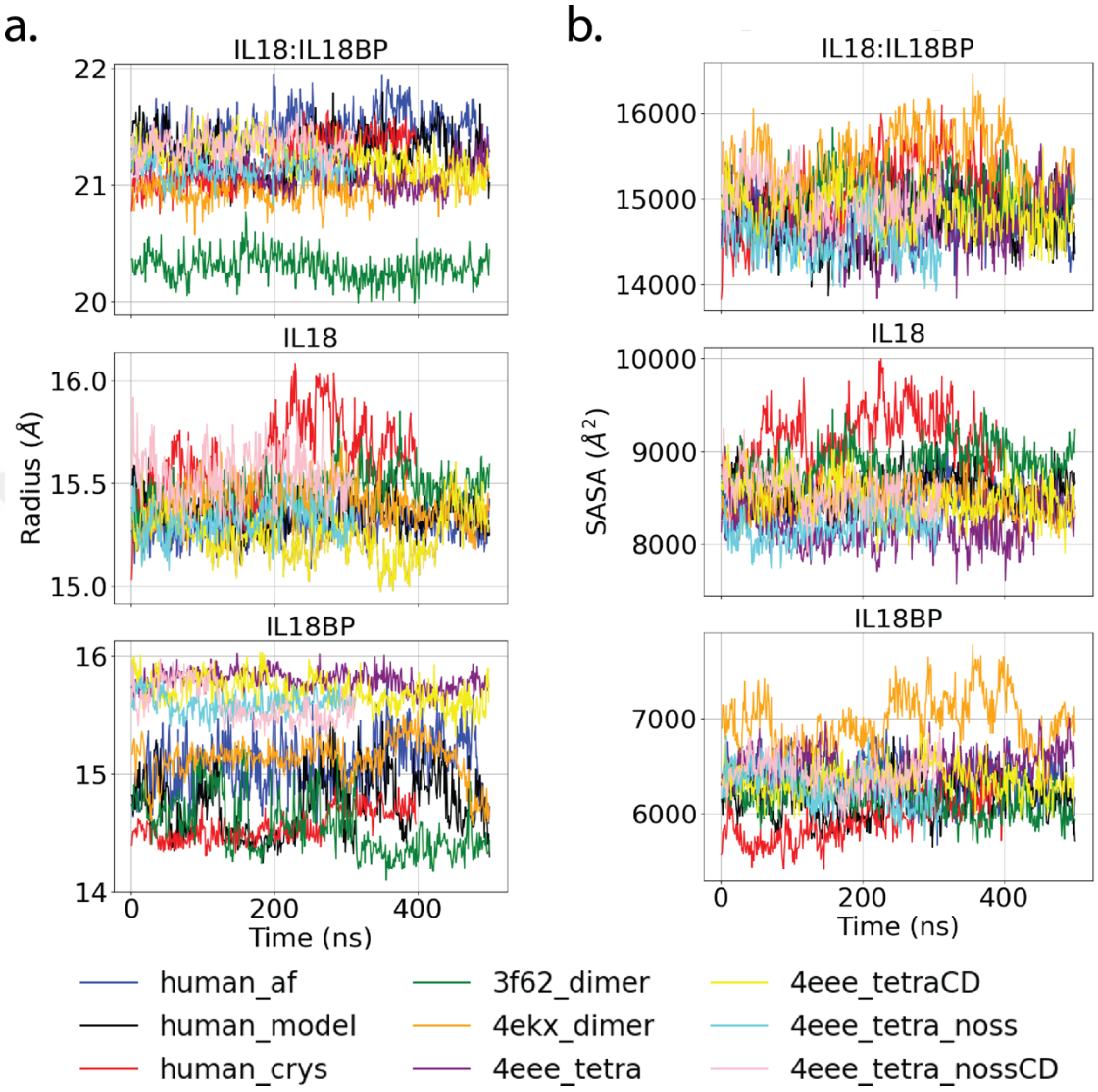

Figure 3.5 The R_g and SASA plots of all models. The R_g and SASA indicate the compactness ad stability of the molecule for IL18-IL18BP complex, IL18, and IL18BP. af: AlphaFold2, model: homology model, crys: crystal, tetra: tetramer, CD: C-D chain, noss: no S-S (Adapted from Yazıcı YY et al., 2023 [98])

3.3 Mobility of IL18 is dependent on the conformation of the small surface epitope

The Cα-RMSF measurements of all available IL18-IL18BP complexes were calculated using the last 200 nm of simulation (Figure 3.6a). The RMSF changes on the exterior side or tail were excluded from interpretation. The results showed that one region in the IL18 displayed fluctuation, whereas two regions in the IL18BP showed fluctuation throughout the simulation (Figure 3.6a, I). Notably, region I in the IL18 protein is the same region where the small surface epitope of interest resides (Figure 3.1c). The other fluctuated region found in the IL18BP are named DE and EF loops, respectively [76].

If all models were compared for the fluctuation in region I, only computed models displayed fluctuation to a lesser extent (Figure 3.6a). The flexible region I in the computed models remained very stable throughout the simulation as the average fluctuation is calculated as 2 Å in the computed model. The computational models remained stable and compact throughout the simulation as no parts of the complex showed high levels of fluctuation except the C-terminal of IL18BP (Figure 3.6a). On the other hand, both viral and human models exhibited higher fluctuation in region II and region III, respectively (Figures 3.6a and 3.8).

The essential dynamics and configuration of the complex throughout the simulation were investigated using the PCA and FEL analysis by using the 200 nm of each model (Figure 3.7). To describe the essential dynamics of the IL18-IL18BP complexes, the first two PCs representing at least 40% of the variance in most of the subunits of the models were considered. The overall results of the PCA calculations indicate that IL18 and IL18BP remained stable in the confined space, with few exceptions, without a major change. The

wide PC1 and PC2 axes were observed for the IL18 in the human crystal and ectromelia virus models (Figure 3.7). However, FEL plots revealed that the ectromelia virus model remained in one configuration, while the human crystal displayed a larger change in conformation and space considering the wide PC1 axes. We also observed wide PC1-PC2 axes in the IL18BP for nearly all complexes. The C-terminal fluctuation of the IL18BP might affect the PCA calculation as the FEL plot shows one dominant configuration for all heterodimer complexes (Figure 3.6). Additionally, RMSF and essential dynamics analyses also showed that the tetrameric structures were not destabilized by the removal of the intermolecular disulfide contacts. The tetramer molecules showed no difference and rigid backbone with or without the intermolecular disulfide contacts (Figures 3.6, 3.7 and 3.8)

We performed dPCA to explore the configuration and conformation changes that occurred during the MD simulation. The dihedral angles ϕ and ψ of the residues contain more information compared to the cartesian coordinate of the residues [102,103]. Because the dihedral angles are not linear, taking the cos and sin of the dihedral angles provide linearity to calculate PCA. The calculation of the dPCA by cos and sin operation on IL18 and IL18BP was not conclusive, as the first two PCA components represented only 3% of the overall variance. The limited mobility on the protein backbone was also reflected in the poor dPCA variance (see Appendix). Without the transformation, the dPCA represents 30-40% of the variance. The results obtained from the PCA and dPCA were mostly similar. While we observed high levels of fluctuation in the 7al7 protein, the overall structure remained stable. FEL results from both PCA and dPCA of 7al7 showed the possibility of three configurations. However, we can see improvement in the dPCA results since we can observe one dominant minimum representing the stable backbone

of 7al7 throughout the simulation. (Figure 3.9). The PCA of the YLDV tetramer complex with or without a disulfide bridge illustrated different results for the different chains (Figures 3.9 and 3.10). Without the disulfide bridge, one of the heterodimers of IL18 and IL18BP tetramer displayed two different minima (Figure 3.9). Considering the dPCA FEL analysis of tetramer, the disulfide bridge seems to be not affecting the overall configuration, as previously noted. However, the difference between the RMSDs with and without the disulfide bridge may be reasonable, as one heterodimer chain of the tetramer without disulfide showed two minima in the dPCA FEL (Figures 3.9 and 3.10). It should be noted that the first two components of dPCA were still not sufficient to represent all configurations due to low variance.

The dPCA analysis was performed for the small surface region containing 10 residues and the five residues within this small surface region including Ser, Asp, Cys, Arg, and Asp. The dPCA analysis with transformation still did not result in a high variance in the first 5 PCA components (Figure 3.11). However, limiting the number of residues to five led to increased variance for the region (Figure 3.12). The fluctuation of the cysteine was of interest. Thus, surrounding amino acids flanking the cysteine were selected for the dPCA. The dPCA FEL without the sin and cos transformation showed only one minimum for the IL18 except for the 4ekx (Figure 3.12). However, after performing dPCA and angular transformation to five residual regions, multiple minima, and possible configurations were noticed for the 7al7 and 4ekx (Figure 3.12). On closer inspection, it can be inferred that in both molecules, a small surface region highly fluctuates, while the 4ekx is more extreme (Figures 3.8 and 3.12). More importantly, dPCA shows the small configuration change and fluctuation that occur within the loop within the closer

inspection (Figure 3.12). This result also implies that small surface regions bearing the C74 are flexible and can be found in different conformations within the simulation.

We computed average fluctuations of the human complex using two replicates of the human crystal complex (7al7) and of two computed models (Figure 3.6b). Mean fluctuations were generally higher in the crystal complex than the computed models, particularly for the short surface epitope (Figure 3.1c). We also observed high mobility of region III in the decoy crystal structure of the human complex. The human tetramer, which was constructed using the 7al7 heterodimer, showed particularly low mobility compared to the heterodimer form (Figure 3.6b). Although both heterodimer and tetrameric forms of human complexes shared the same conformation for the short surface epitope encompassing residues from 68 to 81, reduced flexibility of the tetramer is likely to result from the steric effect of tetramerization. Overall, these analyses suggested that the initial conformation of the surface epitope affects the flexibility of region I of IL18 and region III of IL18BP (Figure 3.6).

The two replica systems of the human and computational models were used to calculate the average fluctuations (Figure 3.6b). The average fluctuation of the backbone was lower in the computational model compared to the crystal complex, particularly the short surface region found in the IL18 (Figure 3.1c). The high mobility was observed in region II of the human crystal model compared to other complexes. The human tetramer, which was generated using the heterodimer form of the human crystal IL18-IL18BP complex, displayed higher stability and less flexibility compared to the heterodimer form (Figure 3.6b). The lower flexibility observed in the tetramer structure may arise from the steric effect of tetramerization as in both heterodimer and homodimer small surface regions that preserved their disordered secondary structure. In conclusion, the initial

configuration of the small surface region on IL18 determines the flexibility of region I of IL18 and region III of IL18BP (Figure 3.6)

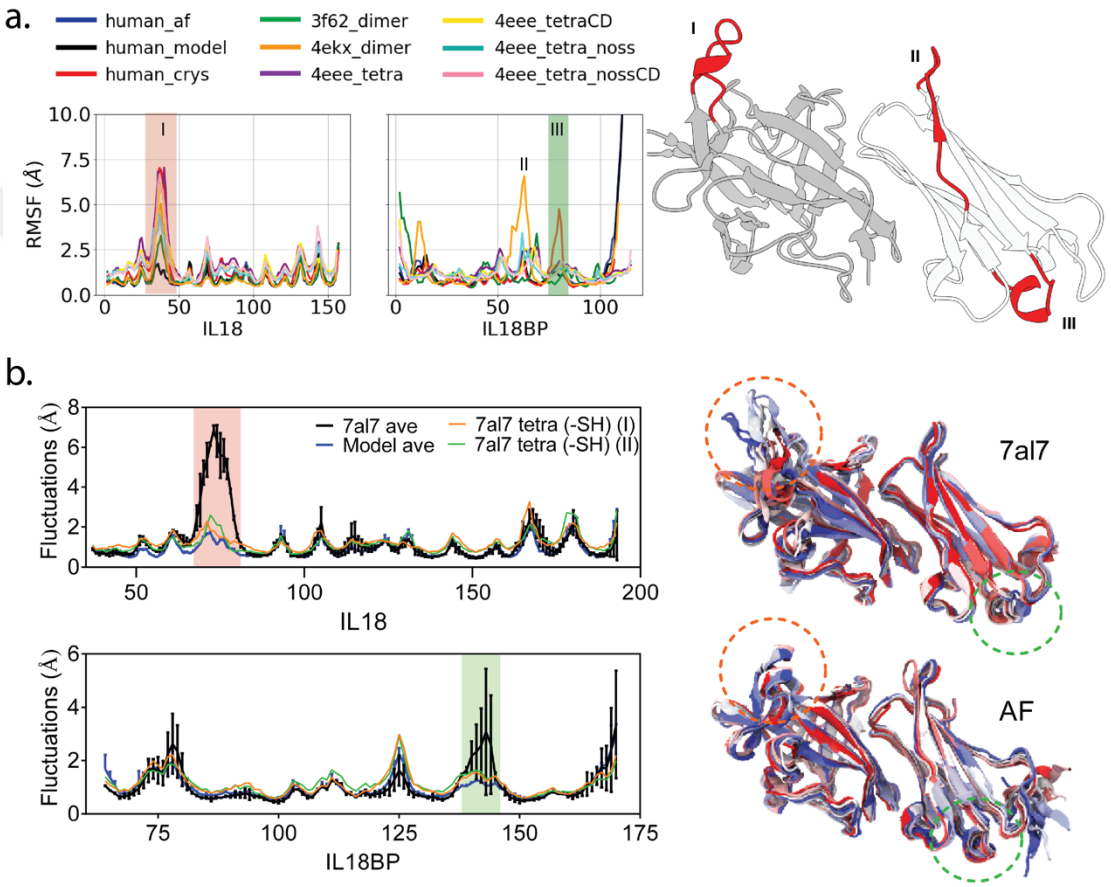

Figure 3.6 RMSF calculation of all models. (a) Panel shows Cα fluctuations calculated for the last 200 ns. Human af (AlphaFold2): blue, human homology model: black, human crystal: red, 3f62: green, 4ekx: orange, 4eee (S-S) A-B chains: purple, 4eee (S-S) C-D chains: yellow, 4eee (-SH) A-B chains: teal, 4eee (-SH) C-D chains: pink. The complex structure illustrates the mobile regions colored red. (b) Average fluctuations of the human complexes for the last 200 ns, crystal structure (black), and computed models (blue). Two replicate simulations were used for both structures, with error bars representing the standard deviation. Fluctuations of the human tetramer were shown in orange and green lines representing each subunit in the 2:2 complex. The residue index was set according to the 7al7 structure. Shaded areas mark highly mobile regions in the reduced trajectory of the dimer structures of crystal complex (7al7) and the AF2 computed model. (Adapted from Yazıcı YY et al., 2023 [98])

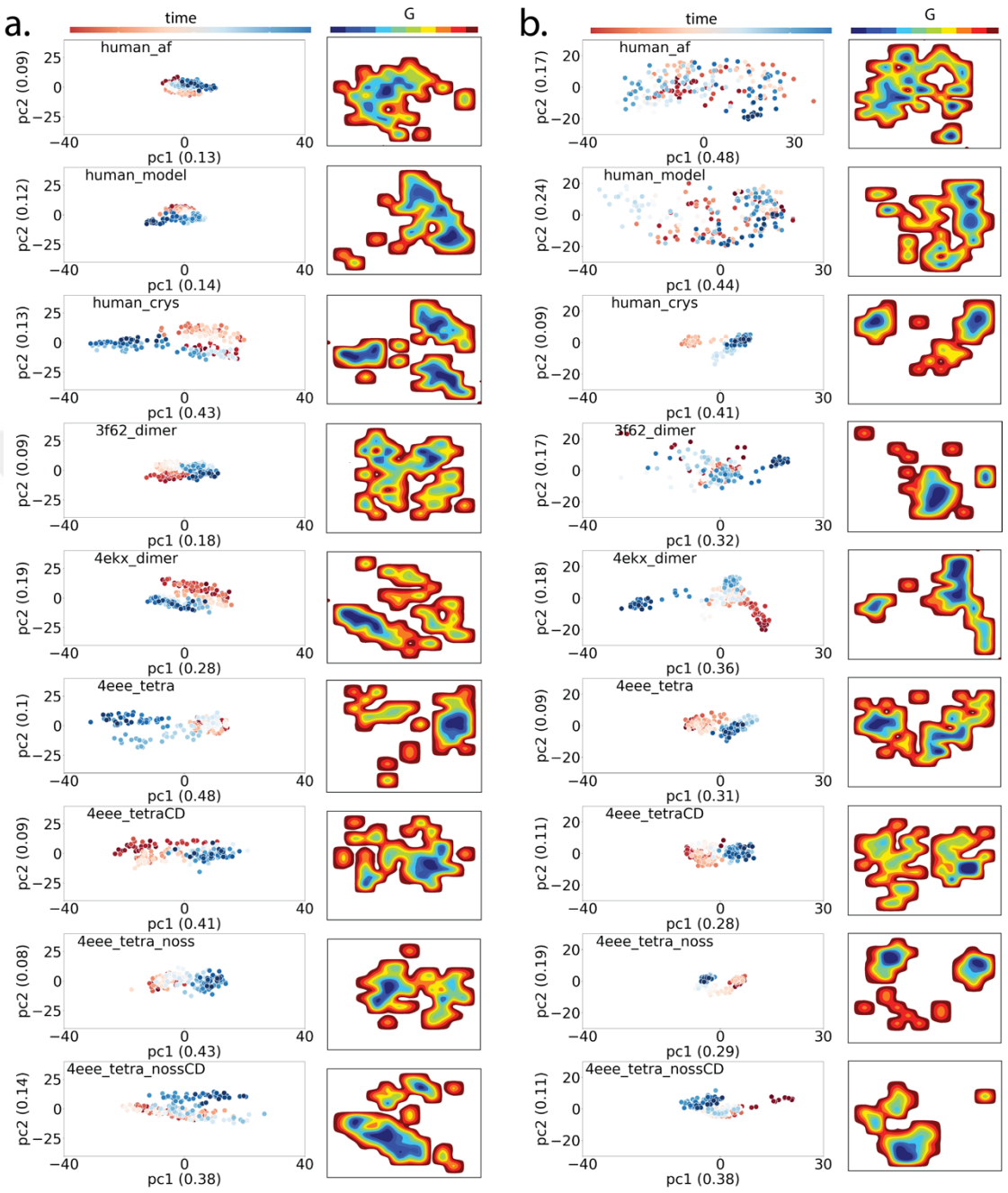

Figure 3.7 Essential dynamics and free energy landscape of human IL18 and IL18BP. Essential dynamics and free energy landscape of human (a) IL18 and (b) IL18BP were analyzed by the first two PCs using the last 200 ns of the production runs. Possible low-energy conformations were extracted by the free energy landscape shown on the right panel. (Adapted from Yazıcı YY et al., 2023 [98])

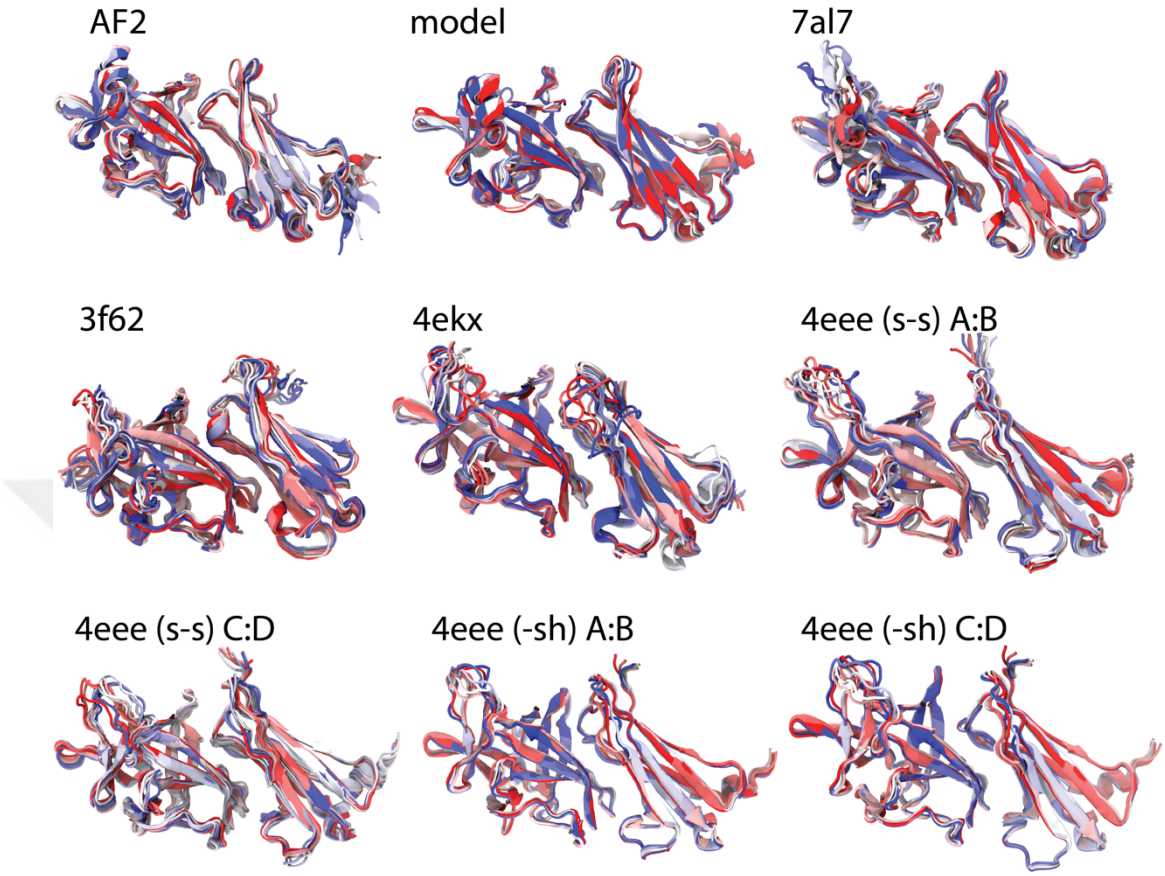

Figure 3.8 Evolution of the complexes throughout the production runs. The red, white, and blue color scales indicate the time points when the snapshots are extracted. Red: start, Blue: end, White: intermediate. (Adapted from Yazıcı YY et al., 2023 [98])

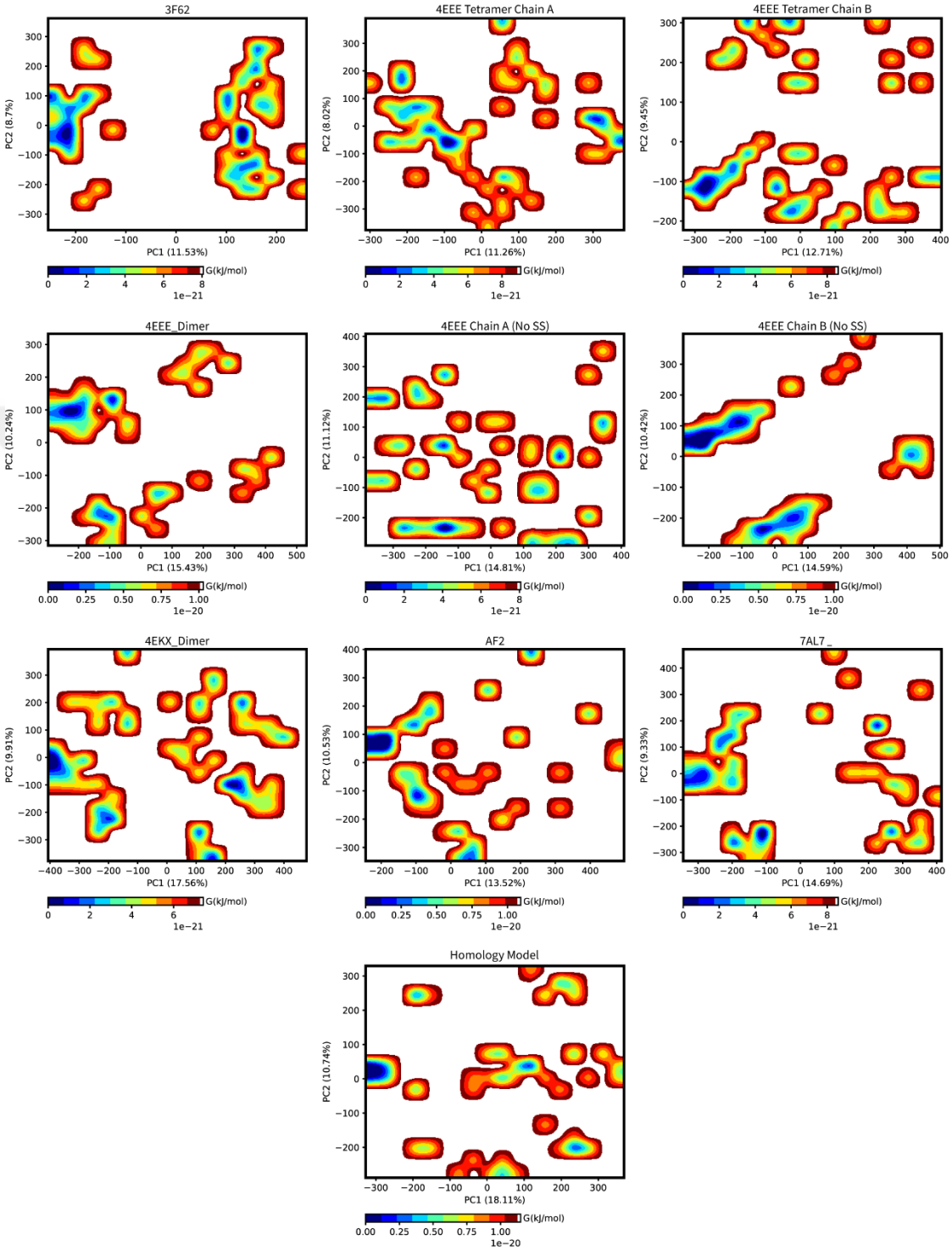

Figure 3.9 Essential dynamics and free energy landscape analysis of IL18 by dPCA. Essential dynamics and free energy landscape of IL18 were analyzed by the first two PCs using the dihedral angle of the last 300 ns of the production runs. Minimum energy areas in the figure indicate possible low-energy structural conformations.

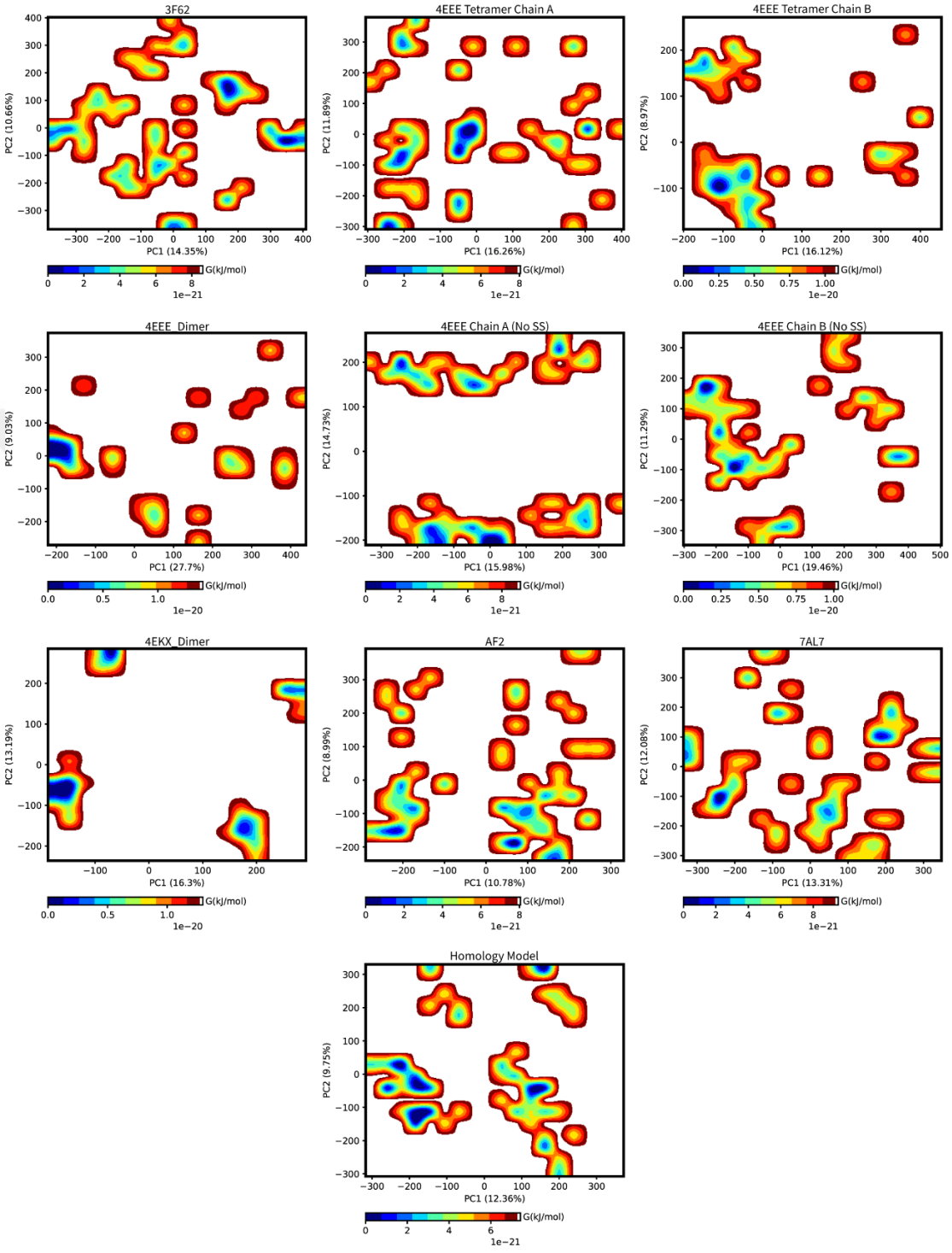

Figure 3.10 Essential dynamics and free energy landscape analysis of IL18BP by dPCA. Essential dynamics and free energy landscape of IL18BP were analyzed by the first two PCs using the dihedral angle of the last 300 ns of the production run. Minimum energy areas in the figure indicate possible low-energy structural conformations.

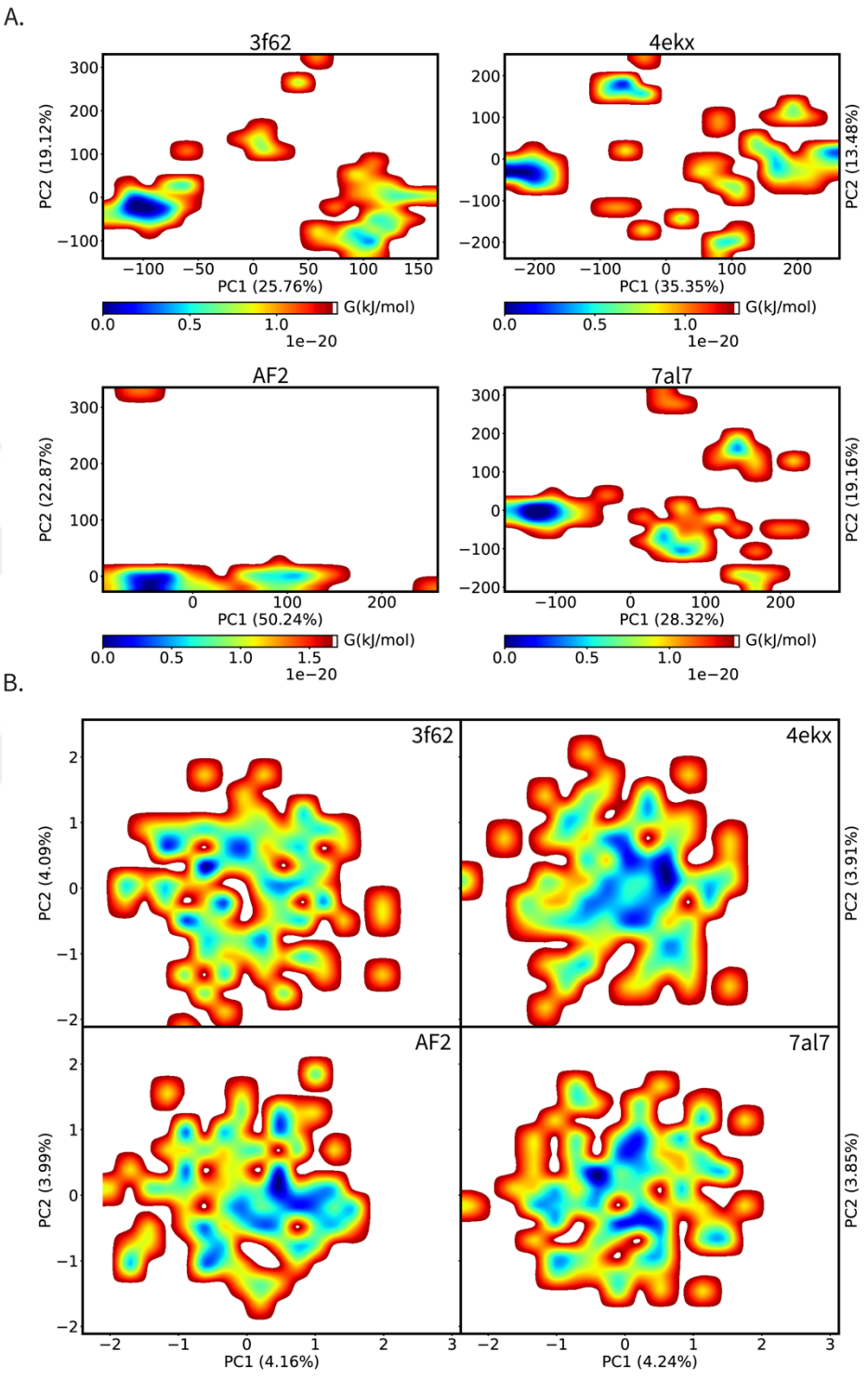

Figure 3.11 Essential dynamics and free energy landscape analysis of small surface region by dPCA. Analysis of small surface epitope in IL18 was performed by the first two PCs using the (a) dihedral angle of the last 300 ns of the production runs and (b) cos and sin transformation of dihedral angle of the last 300 ns of the production runs. Minimum energy areas in the figure indicate possible low-energy structural conformations.

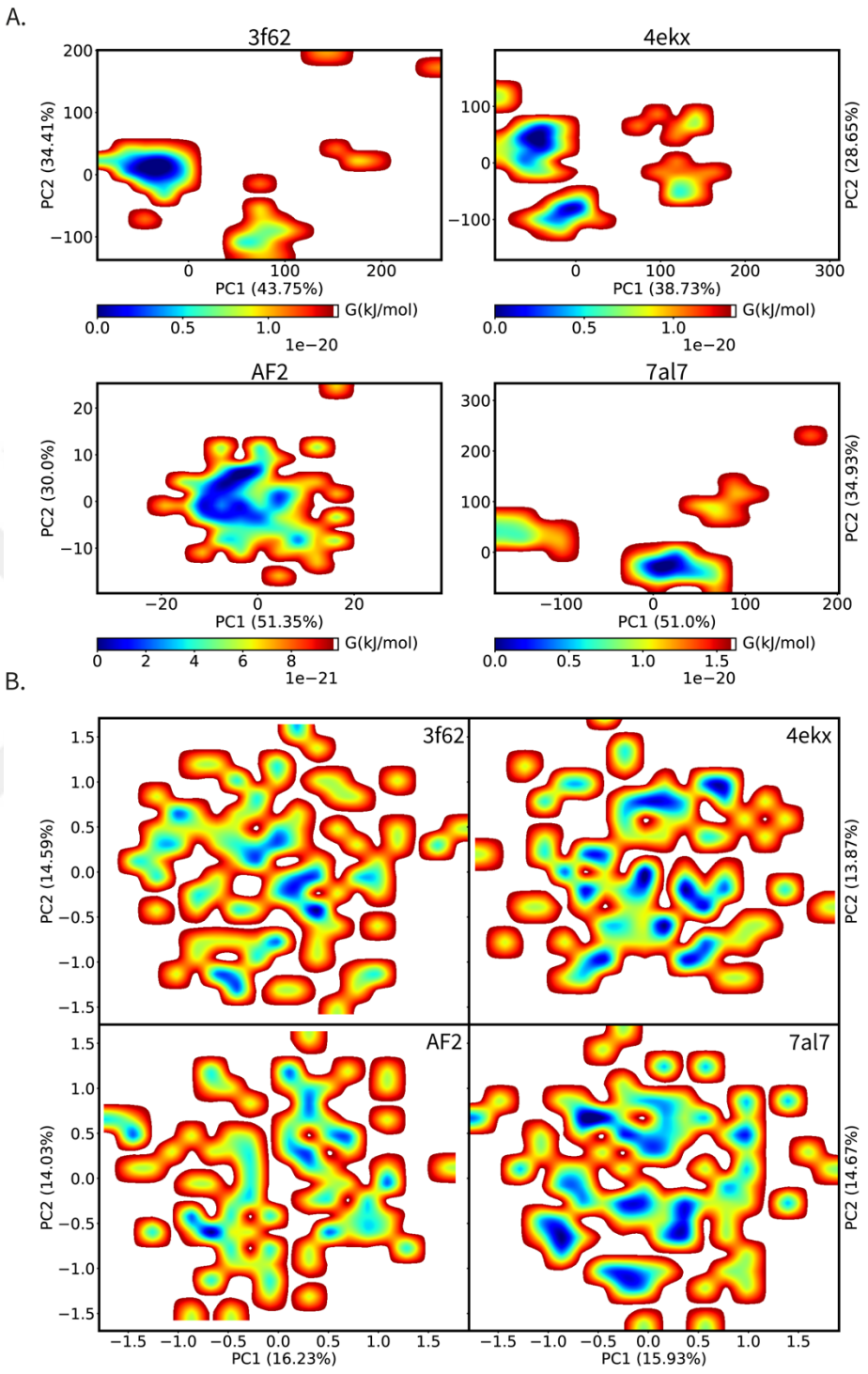

Figure 3.12 Essential dynamics and free energy landscape analysis of cysteine and surrounding residues by dPCA. Analysis of the C74 and surrounding 5 residues on IL18 were done by the first two PCs using the (a) dihedral angle of the last 300 ns of the production runs and (b) cos and sin transformation of dihedral angle of the last 300 ns of the production runs. Minimum energy areas in the figure indicate possible low-energy structural conformations.

3.4 Conformation of the small surface helix mediates stability and self-assembly of heterodimers

The small surface region on IL18 in different IL18-IL18BP complexes was investigated (Figure 3.13). After analyzing the static structure of the IL18 complexes, we found one acidic (E192) and one basic amino acid (R75) in closer proximity if this region folds into the helix (Figure 3.13a). In more details, the guanidinium group of R75 extends towards the carboxylic acid group of E192, while the sidechain of D71 attracts R49, resulting in two salt-bridge interactions in the hIL18 that stabilize and preserve the helical configuration of the small surface region (Figure 3.13). The salt bridge does not exist if the helical structure on the small surface region is disrupted (Figures 3.13a and 3.8). Moreover, AF2 and homology computed models showed similar salt bridge interactions, as both preserve their helical configuration while forming a strong salt bridge between E192 and R75 and one between R49 and D71 to a lesser extent (Figure 3.13b). In conclusion, these finding indicates that the initial configuration of the small surface region of IL18-IL18BP determines the dynamics of the IL18-IL18BP complex. Finally, additional interactions, such as the salt bridges, preserve and stabilize the structure.

The C74, which is found in the region I, is suggested to form a disulfide bond during self-assembly of the IL18-IL18BP heterodimer complex (Figure 3.13a) [76]. In the computational models where the small surface region folds into the helix, C74 is buried and not accessible, evident with that the relative accessible surface area (rASA) was calculated as 0.007 and 0.015 for the AF2 and homology modeling, respectively. In contrast, C74 residue was exposed in the human crystal structure, with a calculated rASA of 0.748. Figure 3.13b displays the evolution of the small surface region through 500 ns

simulation. The small surface region on the computational model remains static and preserved initial configuration, whereas C74 remains completely buried. However, the small surface region on the human crystal extended from its core and did not build any salt bridge interaction during the process (Figure 3.13b).

Figure 3.14a shows the SASA measurement of the 74th amino acid position of the human IL18-IL18BP complex. The C74 was only found in five of the complexes used in this study, while the 74th position of viral complexes was substituted with the serine [75,77]. Regarding maximum accessible surface area (ASA) values of amino acids, a cysteine can reach an average of 150 $Å^2$ and a serine could reach an average of 137 $Å^2$ [108–110]. Considering the maximum ASA measurement obtained from viral and human crystals, the 74th stays accessible except for the computational models (Figure 3.14a). The C74 remaining inside of the helix does not provide the possibility of any possible intermolecular interaction (Figure 3.14a). SASA measurement of the entire region I through simulation was also recorded (Figure 3.14a, bottom). SASA measurement confirms that the small surface region stayed compact and did not expose any cysteine residue, while other models became looser and remained exposed (Figure 3.14a, bottom panel). Finally, SASA was calculated for the C131 on the IL18BP, which is proposed to form a disulfide bond with C74 on hIL18 (Figure 3.14b) [76]. All the models used in the study exhibited partial accessibility and remained unaltered.

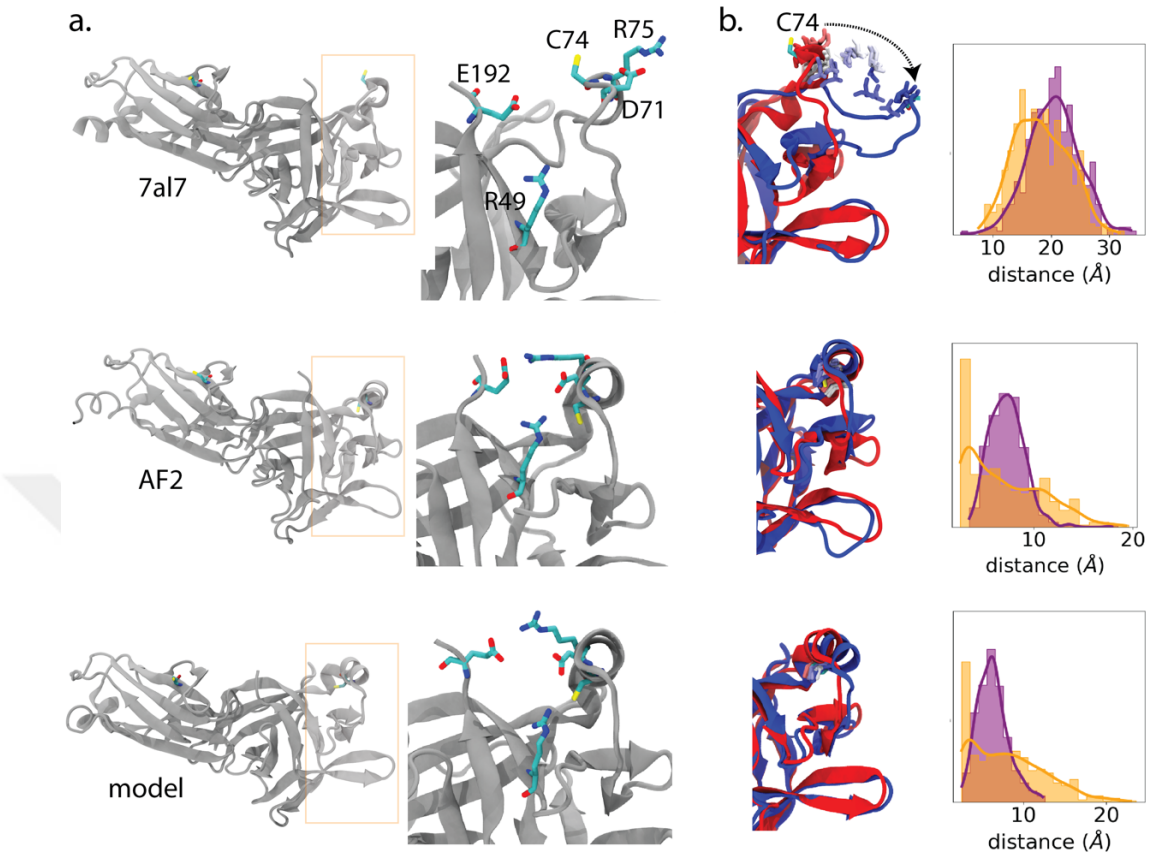

Figure 3.13 Dynamics of the small surface helix in the human complexes. The top panel illustrates the crystal complex, and the bottom panels show the computational models. The movement of the helix/loop is shown in the second column. The red color indicates the starting conformation and the blue shows the conformation after 300 ns. Two salt bridge contacts were shown for the starting structure alongside the C74. Distance distributions of the salt bridges were shown (orange: E192-R75, purple: D71-R49). Residue numbering follows the 7al7 structure. (Adapted from Yazıcı YY et al., 2023 [98])

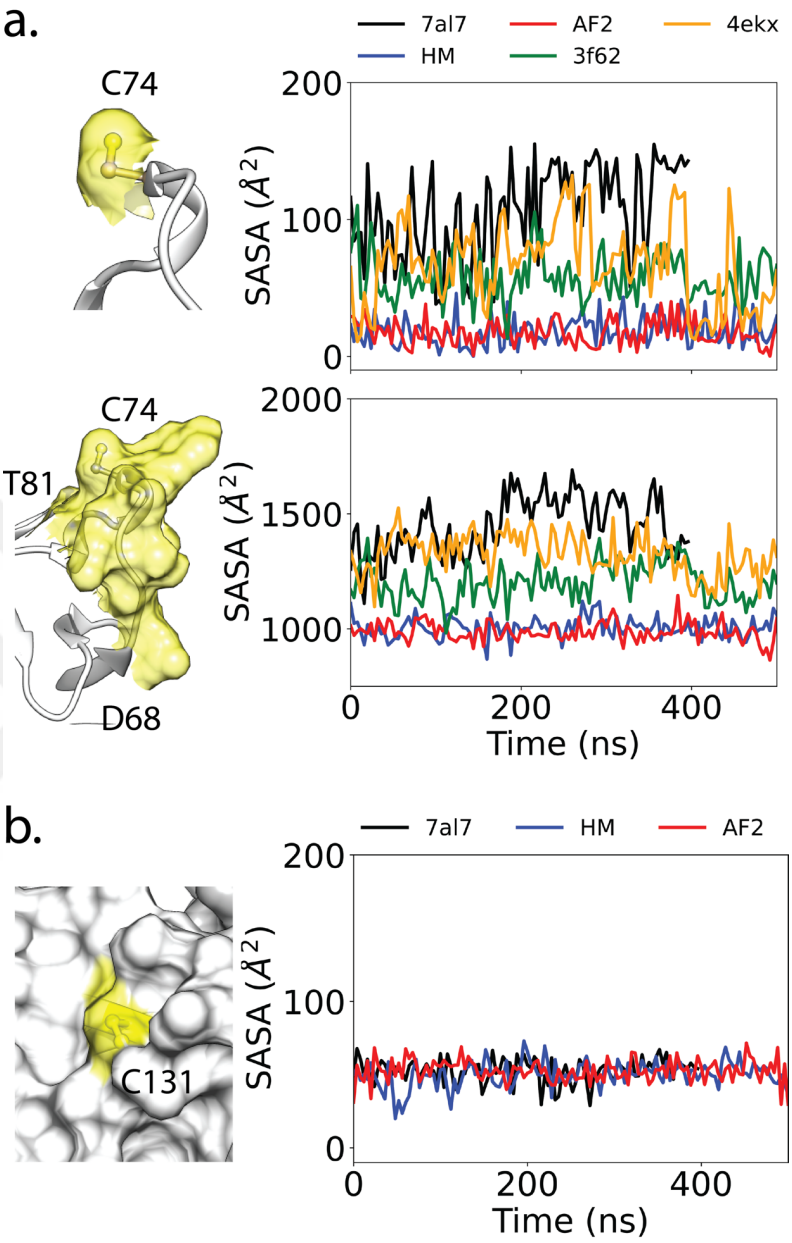

Figure 3.14 SASA changes of the 74th and 131st positions over time. (a) Top panels show the SASA changes of the 74th positions of the hIL18 over time, and bottom panels show the overall SASA of the entire surface region holding this position. (b) Panel shows the SASA changes over time for the C131 of hIL18BP, which was proposed to participate in a novel intermolecular disulfide contact with the C74 of hIL18. (Adapted from Yazıcı YY et al., 2023 [98])

3.5 Human tetramer stability is dependent on intermolecular disulfide bonds and other interactions

The contribution of disulfide bonds was assessed for each tetramer complex by modeling each with or without intermolecular disulfide bond(s) (Figure 3.4b-c). The YLDV IL18-IL18BP tetramer model showed that the disulfide, hydrophobic, and ionic bonds stabilize the tetrameric assembly of the viral model (Figure 3.15b). We measured the R_g of the hydrophobic cluster found in the site consisting of I29, V31, V124, and I129 residues (Figure 3.15c). Additionally, the salt bridges between K34 and D122 and between E35 and R105 were controlled by measuring distance throughout the simulation. YLDV tetramer assembly preserved the distance between the salt bridge and hydrophobic core with or without the disulfide bridge. These findings reduce the importance of the disulfide bridge on YLDV IL18-IL18BP tetramer assembly and point to the other secondary interactions that increase the stability of the complex.

The atomic coordinates of the IL18-IL18BP tetramer assembly were not available. Hence, the human IL18-IL18BP tetrameric assembly was built by using the two 7al7 heterodimers. The construct was equilibrated with two disulfide bonds between C74 of hIL18 and C131 of hIL18BP. The in-silico constructed tetramer showed a sudden change in its conformation and then became stable throughout the simulation (Figure 3.4c). Then, we extracted a snapshot from the stabilized trajectory and removed disulfide contact (Figure 3.4c). Despite cysteine modeled as a reduced state (-SH), human tetramer preserved its stability and subunits remained intact (Figure 3.4c). Further investigation of the cysteine interface revealed that only one cysteine pair remained after the disruption of the disulfide bond (Figure 3.16, blue). However, the other pair began to split up and

the interface was abolished (Figure 3.16, orange). Similar to the YLDV tetramer, E105 of hIL18 and R113 of IL18BP interact with each other during tetramer assembly and stabilize the structure (Figure 3.16).

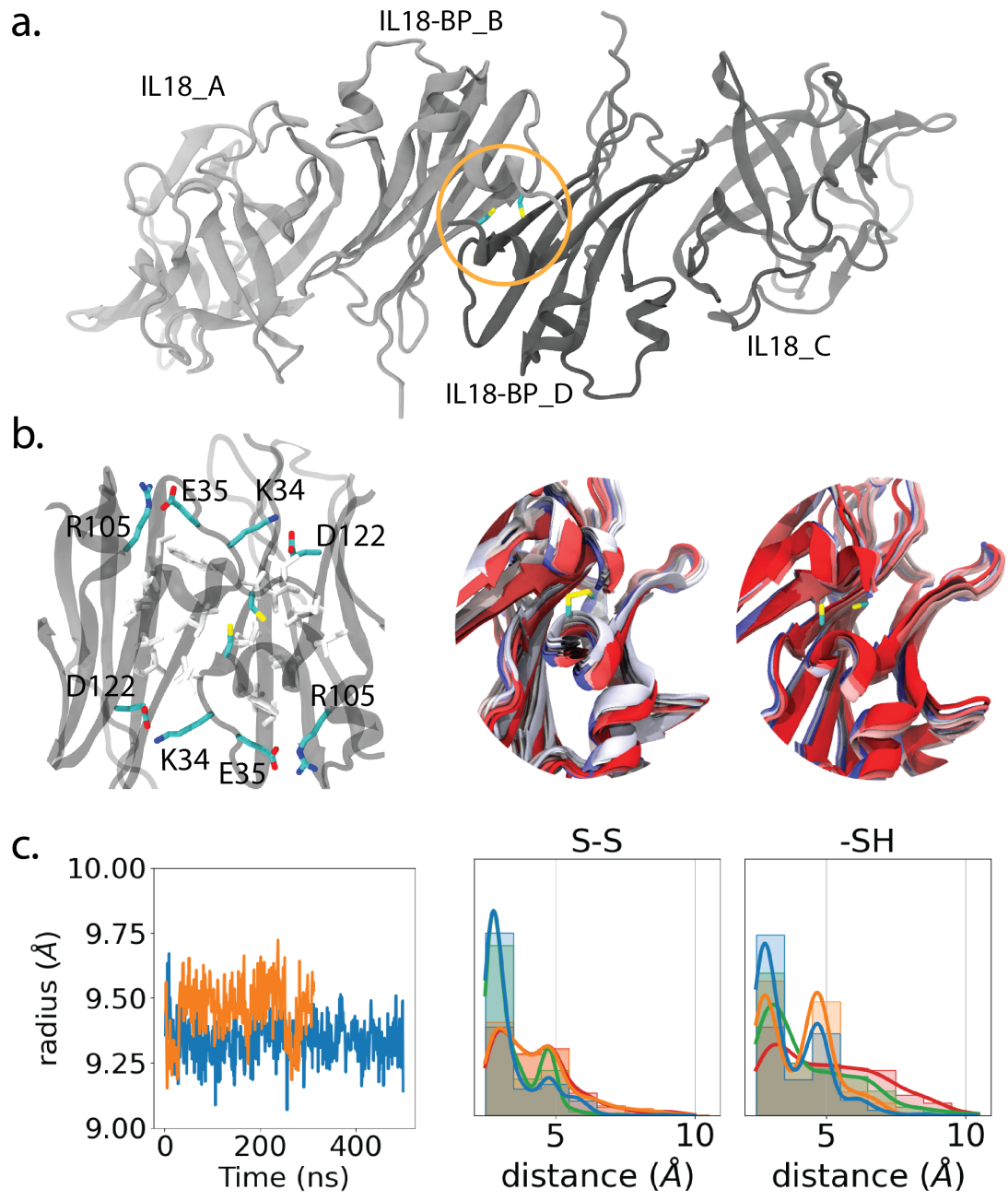

Figure 3.15 YLDV (4eee) tetramer assembly. (a) Panel shows the tetrameric 2:2 complex (4eee) marking the intermolecular disulfide bridge between the IL18BP chains. (b) Panel shows the interface between IL18BP chains. Two disulfide bridges (E35-R105, K34-D122) were spotted for both chains. Surrounding hydrophobic amino acids were shown by white stick models. The reduced trajectory was shown for the IL18BP symmetric interface in the presence (S-S) and absence (-SH) of the intermolecular disulfide bridge (C132-C132). (c) Analysis of the radii of the hydrophobic residues at the interface shown in b and analysis of distance distributions of the salt bridges (E35-R105: orange, red; K34-D122: green, blue). (Adapted from Yazıcı YY et al., 2023 [98])

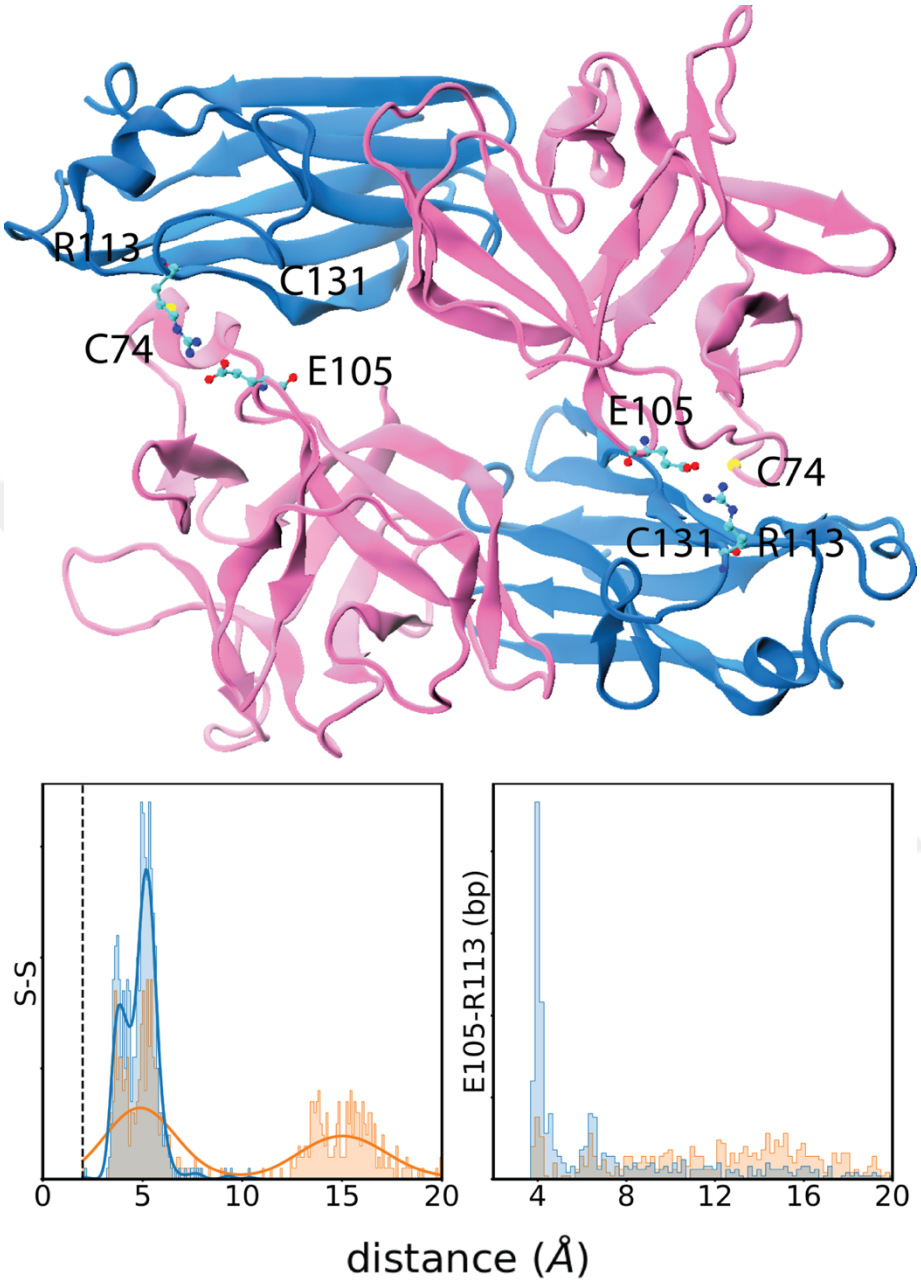

Figure 3.16 Tetramer structure of human IL18 and IL18BP complex. Tetramer structure of IL18 (pink) and IL18BP (blue) complex is shown, highlighting two symmetric ionic interactions between E103 and R113. Distance distributions of two cysteine and these ionic interactions were plotted for the entire trajectory. Orange and blue colors mark the left and right interfaces, respectively. (Adapted from Yazıcı YY et al., 2023 [98])

CHAPTER 4

Discussion

Based on the quaternary structures of the IL18 complexes, the small surface epitope containing the residues between 68 and 81 in the IL18 is either unfolded or missing in all known IL18-IL18BP complexes [73,75–77]. Conversely, a 3_{10} helical conformation dominates in other IL18 structures including those in the free form or in the IL18 signaling complex [53] (Figure 3.1). This surface region does not reside within the binding interface between the IL18 and IL18BP heterodimer. However, a small surface epitope is located at the binding interface of the IL18-IL18Rα complex, suggesting the importance of the epitope in the formation of the binary signaling complex [53]. Additionally, this region contains the C74 amino acid that is reported to form a novel intermolecular disulfide bond in human tetramer [76]. This small surface epitope in known crystal structures of the IL18-IL18BP complex has been recognized, however there is no information regarding the dynamic movement or interaction within the IL18-IL18BP complexes, and how these movements are influenced by small surface epitopes [111]. Hence, this study provides a detailed investigation of the conformational space of the small surface region and its influence on the stability of heterodimer and tetramer assemblies through MD simulations. All structures except the computational models showed fluctuations and flexibility for the small surface epitope in the IL18, indicating that the initial configuration of the small surface impacts on the dynamics of the IL18-IL18BP complex. The small surface epitope of computational models exhibited minuscule movement and flexibility except for the C-

terminal of IL18BP (Figure 3.6). The model obtained from AF2 contains a little longer (~5 amino acids) C-terminal compared to experimental models [76]. The predicted region is depicted as a poor estimation based on the low confidence score annotated by AF2 (Figure 3.1a). The high mobility of computational models in the C-terminal arose from the disordered nature of the structure, which is indicated by the low confidence assigned by AF2 [112,113].

The small surface region in the hIL18 from nine PBDs (3wo2, 3wo3, 3wo4, 2vxt, 4hjj, 4r6u, 4xfs, 4xft, and 4xfu) exhibited a compact 3_{10} helical conformation containing residues between 68 and 81. The small surface region conformation for the remaining PDBs is absent (7al7, 3f62, 4eee, 4ekx) or flexible (1j0s) [33]. IL18 adopts a helical folded structure for the small surface region in the PDBs of the receptor complex and resides in the interface between IL18 and IL18Rα [53]. It should be noted that all small surface epitopes obtained from the IL18-IL18BP complexes demonstrate disordered structure, which is also found within the active binding interface between IL18 and IL18Rα [53], implying that the allosteric effect might lead to the unfolding of the small surface epitope. Allosteric changes in the structure of the protein are the common mechanism to regulate the protein-protein interaction [114,115]. Because the C74 is also found within the surface epitope, the disulfide bond might be an allosterically regulated disulfide bond in the human tetramer complex [116]. However, the simulations used in the study were not able to reinforce the assumption, as the 3_{10} helical structure persistently preserved and displayed high stability (Figure 3.6b). However, conventional MD techniques used in the study might not create possible configurations through simulation as they may not be adequate at sampling to observe allosteric changes [117]. Hence, enhanced sampling

methods might be a useful alternative to investigate a potential conformational change that occurs on the small surface epitope [117,118].

Self-assembly of the IL18-IL18BP heterodimers can be an alternative mechanism to enhance the inhibition of the IL18 activity for the host and viral decoy [73]. Up to present, two tetramers assembled by the heterodimers of hIL18 with YLDV and human IL18BPs have been discovered. In both self-assemblies, intermolecular disulfide bonds are reported to play an important role in the assembly of tetramer complexes, as the disulfide bonds are known to increase stability and regulate the protein function [119]. However, among two tetramers, only the YLDV tetramer structure was captured by crystallization, whereas the human tetramer structure was predicted to form a symmetry-related assembly based on non-reducing Sodium dodecyl sulphate-Polyacrylamide gel electrophoresis (SDS-PAGE) analysis [76]. It has been known that disulfide bonds can be established by the first folding event of the protein to provide stability and remain stable until the protein degradation occurs, whereas the other alternative is that disulfide bonds can create the reversible dynamic change necessary for the activity of the protein [116,120]. The disulfide bond between C74 of IL18 and the C131 of IL18BP is likely to be dynamically constructed. Our simulation revealed that C74 appears to be fully accessible after the dynamic changes occur in the IL18 of the human crystal during MD simulation of the IL18-IL18BP complex. During constant dynamic movement of the surface epitope of human crystal in the MD simulation, surface epitope between 68 and 81 emerged as more exposed than crystal structure in some of the configurations, demonstrating the crucial role of the small surface region in the tetramer assembly of the IL18-IL18BP [76].

Multivalent binding is a reversible binding strategy that increases the affinity and specificity of the protein complex in the immune system [121–123]. Human and the YLDV

decoys use this strategy to increase the inhibition and regulation of the hIL18 by the cysteine residue on their surface. Comparison between viral and human IL18BP amino acid sequences and different positioning of the cysteine through different surfaces may imply the possibility of different self-assembly varieties of the heterodimer complex. Human tetramer is found within grid shape symmetric geometry to form assembly with the help of the disulfide bond between IL18 and IL18BP. In contrast, the YLDV tetramer complex formed upon the disulfide bridge between C132 of IL18BPs results in the positioning of both dimers side-by-side. YLDV tetramer is also supported by the additional intermolecular interactions apart from the disulfide bond. The hydrophobic amino acid group and the additional four symmetric salt bridges increased the stability of the tetramer complex, as the interface was not disrupted even after the breakage of the disulfide bond. Although the hydrophobic cluster in the tetramer complex has been studied by a mutagenesis analysis, the contribution of the salt bridge to the stability of the tetramer was revealed by this study [73].

In this study, the human self-assembly formed a novel salt bridge interaction between the E105 of IL18 and the R113 of IL18BP in the tetramer complex (Figure 3.16). However, the breakage of the disulfide bond in the human tetramer resulted in the disruption of only one side of the interface. Nevertheless, the salt bridge between two subunits requires the intact disulfide bond, as breaking the disulfide bond results in the loss of the salt bridge. Comparison between two tetramers of human and YLDV suggests that the human tetramer is less stable and contains fewer contacts in the interface (Figure 3.15b-c). However, breakage of the disulfide bridge and disruption of the one side of the interface did not result in the disruption of the tetramer. Hence, the bivalent binding mode of the human tetramer may provide a stability advantage (Figure 3.16, orange densities). Altogether,

one interface in the tetramer complex remained unchanged even after the destruction of the other interface. Hence, the bivalent binding mechanism of grid-like organized human tetramer increases stability, compared to the heterodimer form with the unfolded small surface epitope.

CHAPTER 5

Conclusion and Future Perspectives

In conclusion, AF2 and homology prediction gave an accurate representation of the human IL18-IL18BP complex, implying the strength of both template-free and template-based method for accurate prediction of the human heterodimer. The conformation of the small surface region on the IL18 is dependent on the source of the hIL18 and hIL18BP. The small surface region maintained its helical fold throughout the MD simulations, reflecting the contribution of this region to the stability of the IL18-IL18BP at the helical fold. Unfolding of this small surface region leads to more flexible hIL18 backbone in the heterodimer. Nonetheless, this surface region when fully unfolded extends towards another IL18-IL18BP heterodimer to form an intermolecular disulfide bridge through the C74. Thus, this surface region plays an important role in the regulation of IL18 activity through affecting the IL18-IL18BP heterodimer dynamics and self-assembly. Possible allosteric regulation recruiting the same short epitope of hIL18 can be further studied by enhanced sampling methods that could more effectively sample and access such conformational transitions. This thesis provides structural insights into the IL18-IL18BP dynamics of the IL18-IL18BP heterodimers and their self-assembly. Altogether these insights could be used to tailor the properties of the recombinant IL18BPs for an effective inhibition of hIL18.

REFERENCES

1. Dinarello, C., Novick, D., Kim, S., & Kaplanski, G. (2013). Interleukin-18 and IL-18 Binding Protein. *Frontiers in Immunology*, *4*. https://www.frontiersin.org/articles/10.3389/fimmu.2013.00289

2. Dinarello, C. A. (2009). Immunological and inflammatory functions of the interleukin-1 family. *Annual Review of Immunology*, *27*, 519–550. https://doi.org/10.1146/annurev.immunol.021908.132612

3. Ihim, S. A., Abubakar, S. D., Zian, Z., Sasaki, T., Saffarioun, M., Maleknia, S., & Azizi, G. (2022). Interleukin-18 cytokine in immunity, inflammation, and autoimmunity: Biological role in induction, regulation, and treatment. *Frontiers in Immunology*, *13*. https://www.frontiersin.org/articles/10.3389/fimmu.2022.919973

4. Kaplanski, G. (2018). Interleukin-18: Biological properties and role in disease pathogenesis. *Immunological Reviews*, *281*(1), 138–153. https://doi.org/10.1111/imr.12616

5. Novick, D., Kim, S., Kaplanski, G., & Dinarello, C. A. (2013). Interleukin-18, more than a Th1 cytokine. *Seminars in Immunology*, *25*(6), 439–448. https://doi.org/10.1016/j.smim.2013.10.014

6. Belkaya, S., Michailidis, E., Korol, C. B., Kabbani, M., Cobat, A., Bastard, P., Lee, Y. S., Hernandez, N., Drutman, S., de Jong, Y. P., Vivier, E., Bruneau, J., Béziat, V., Boisson, B., Lorenzo-Diaz, L., Boucherit, S., Sebagh, M., Jacquemin, E., Emile, J.-F., … Casanova, J.-L. (2019). Inherited IL-18BP deficiency in human fulminant viral hepatitis. *Journal of Experimental Medicine*, *216*(8), 1777–1790. https://doi.org/10.1084/jem.20190669

7. Chen, O., Shan, N., Zhu, X., Wang, Y., Ren, P., Wei, D., & Sun, R. (2013). The imbalance of IL-18/IL-18BP in patients with systemic juvenile idiopathic arthritis. *Acta Biochimica et Biophysica Sinica*, *45*(4), 339–341. https://doi.org/10.1093/abbs/gmt007

8. Park, S. Y., Hisham, Y., Shin, H. M., Yeom, S. C., & Kim, S. (2022). Interleukin-18 Binding Protein in Immune Regulation and Autoimmune Diseases. *Biomedicines*, *10*(7), 1750. https://doi.org/10.3390/biomedicines10071750

9. Yasuda, K., Nakanishi, K., & Tsutsui, H. (2019). Interleukin-18 in Health and Disease. *International Journal of Molecular Sciences*, *20*(3), 649. https://doi.org/10.3390/ijms20030649

10. Nakanishi, K., Yoshimoto, T., Tsutsui, H., & Okamura, H. (2001). Interleukin-18 regulates both Th1 and Th2 responses. *Annual Review of Immunology*, *19*, 423–474. https://doi.org/10.1146/annurev.immunol.19.1.423

11. Koyama, N., Hoelzer, D., & Ottmann, O. G. (2004). Regulation of human IL-18 gene expression: Interaction of PU.1 with GC-box binding protein is involved in human IL-18 expression in myeloid cells. *European Journal of Immunology*, *34*(3), 817–826. https://doi.org/10.1002/eji.200324420

12. Harel, M., Girard-Guyonvarc'h, C., Rodriguez, E., Palmer, G., & Gabay, C. (2020). Production of IL-18 Binding Protein by Radiosensitive and Radioresistant Cells in CpG-

Induced Macrophage Activation Syndrome. *The Journal of Immunology*, *205*(4), 1167–1175. https://doi.org/10.4049/jimmunol.2000168

13. Bufler, P., Gamboni-Robertson, F., Azam, T., Kim, S.-H., & Dinarello, C. A. (2004). Interleukin-1 homologues IL-1F7b and IL-18 contain functional mRNA instability elements within the coding region responsive to lipopolysaccharide. *Biochemical Journal*, *381*(Pt 2), 503–510. https://doi.org/10.1042/BJ20040217

14. Alsaleh, G., Suffert, G., Semaan, N., Juncker, T., Frenzel, L., Gottenberg, J.-E., Sibilia, J., Pfeffer, S., & Wachsmann, D. (2009). Bruton's tyrosine kinase is involved in miR-346-related regulation of IL-18 release by lipopolysaccharide-activated rheumatoid fibroblast-like synoviocytes. *Journal of Immunology (Baltimore, Md.: 1950)*, *182*(8), 5088–5097. https://doi.org/10.4049/jimmunol.0801613

15. Rex, D. A. B., Agarwal, N., Prasad, T. S. K., Kandasamy, R. K., Subbannayya, Y., & Pinto, S. M. (2020). A comprehensive pathway map of IL-18-mediated signalling. *Journal of Cell Communication and Signaling*, *14*(2), 257–266. https://doi.org/10.1007/s12079-019-00544-4

16. Bossaller, L., Chiang, P.-I., Schmidt-Lauber, C., Ganesan, S., Kaiser, W. J., Rathinam, V. A. K., Mocarski, E. S., Subramanian, D., Green, D. R., Silverman, N., Fitzgerald, K. A., Marshak-Rothstein, A., & Latz, E. (2012). Cutting edge: FAS (CD95) mediates noncanonical IL-1β and IL-18 maturation via caspase-8 in an RIP3-independent manner. *Journal of Immunology (Baltimore, Md.: 1950)*, *189*(12), 5508–5512. https://doi.org/10.4049/jimmunol.1202121

17. Tsutsui, H., Matsui, K., Okamura, H., & Nakanishi, K. (2000). Pathophysiological roles of interleukin-18 in inflammatory liver diseases. *Immunological Reviews*, *174*, 192–209. https://doi.org/10.1034/j.1600-0528.2002.017418.x

18. Sugawara, S., Uehara, A., Nochi, T., Yamaguchi, T., Ueda, H., Sugiyama, A., Hanzawa, K., Kumagai, K., Okamura, H., & Takada, H. (2001). Neutrophil proteinase 3-mediated induction of bioactive IL-18 secretion by human oral epithelial cells. *Journal of Immunology (Baltimore, Md.: 1950)*, *167*(11), 6568–6575. https://doi.org/10.4049/jimmunol.167.11.6568

19. Omoto, Y., Tokime, K., Yamanaka, K., Habe, K., Morioka, T., Kurokawa, I., Tsutsui, H., Yamanishi, K., Nakanishi, K., & Mizutani, H. (2006). Human mast cell chymase cleaves pro-IL-18 and generates a novel and biologically active IL-18 fragment. *Journal of Immunology (Baltimore, Md.: 1950)*, *177*(12), 8315–8319. https://doi.org/10.4049/jimmunol.177.12.8315

20. Omoto, Y., Yamanaka, K., Tokime, K., Kitano, S., Kakeda, M., Akeda, T., Kurokawa, I., Gabazza, E. C., Tsutsui, H., Katayama, N., Yamanishi, K., Nakanishi, K., & Mizutani, H. (2010). Granzyme B is a novel interleukin-18 converting enzyme. *Journal of Dermatological Science*, *59*(2), 129–135. https://doi.org/10.1016/j.jdermsci.2010.05.004

21. Brossart, P., Grünebach, F., Stuhler, G., Reichardt, V. L., Möhle, R., Kanz, L., & Brugger, W. (1998). Generation of functional human dendritic cells from adherent peripheral blood monocytes by CD40 ligation in the absence of granulocyte-macrophage colony-stimulating factor. *Blood*, *92*(11), 4238–4247.

22. Okamura, H., Tsutsi, H., Komatsu, T., Yutsudo, M., Hakura, A., Tanimoto, T., Torigoe, K., Okura, T., Nukada, Y., & Hattori, K. (1995). Cloning of a new cytokine that induces IFN-gamma production by T cells. *Nature*, *378*(6552), 88–91. https://doi.org/10.1038/378088a0

23. Stoll, S., Müller, G., Kurimoto, M., Saloga, J., Tanimoto, T., Yamauchi, H., Okamura, H., Knop, J., & Enk, A. H. (1997). Production of IL-18 (IFN-gamma-inducing factor) messenger RNA and functional protein by murine keratinocytes. *Journal of Immunology (Baltimore, Md.: 1950)*, *159*(1), 298–302.

24. Udagawa, N., Horwood, N. J., Elliott, J., Mackay, A., Owens, J., Okamura, H., Kurimoto, M., Chambers, T. J., Martin, T. J., & Gillespie, M. T. (1997). Interleukin-18 (interferon-gamma-inducing factor) is produced by osteoblasts and acts via granulocyte/macrophage colony-stimulating factor and not via interferon-gamma to inhibit osteoclast formation. *The Journal of Experimental Medicine*, *185*(6), 1005–1012. https://doi.org/10.1084/jem.185.6.1005

25. Puren, A. J., Fantuzzi, G., & Dinarello, C. A. (1999). Gene expression, synthesis, and secretion of interleukin 18 and interleukin 1β are differentially regulated in human blood mononuclear cells and mouse spleen cells. *Proceedings of the National Academy of Sciences*, *96*(5), 2256–2261. https://doi.org/10.1073/pnas.96.5.2256

26. Robertson, S. E., Young, J. D., Kitson, S., Pitt, A., Evans, J., Roes, J., Karaoglu, D., Santora, L., Ghayur, T., Liew, F. Y., Gracie, J. A., & McInnes, I. B. (2006). Expression and alternative processing of IL-18 in human neutrophils. *European Journal of Immunology*, *36*(3), 722–731. https://doi.org/10.1002/eji.200535402

27. Boraschi, D., & Tagliabue, A. (2013). The interleukin-1 receptor family. *Seminars in Immunology*, *25*(6), 394–407. https://doi.org/10.1016/j.smim.2013.10.023

28. Hirooka, Y., & Nozaki, Y. (2021). Interleukin-18 in Inflammatory Kidney Disease. *Frontiers in Medicine*, *8*, 639103. https://doi.org/10.3389/fmed.2021.639103

29. Nakamura, S., Otani, T., Okura, R., Ijiri, Y., Motoda, R., Kurimoto, M., & Orita, K. (2000). Expression and responsiveness of human interleukin-18 receptor (IL-18R) on hematopoietic cell lines. *Leukemia*, *14*(6), 1052–1059. https://doi.org/10.1038/sj.leu.2401789

30. Yoshimoto, T., Mizutani, H., Tsutsui, H., Noben-Trauth, N., Yamanaka, K., Tanaka, M., Izumi, S., Okamura, H., Paul, W. E., & Nakanishi, K. (2000). IL-18 induction of IgE: Dependence on CD4+ T cells, IL-4 and STAT6. *Nature Immunology*, *1*(2), 132–137. https://doi.org/10.1038/77811

31. Sareneva, T., Julkunen, I., & Matikainen, S. (2000). IFN-alpha and IL-12 induce IL-18 receptor gene expression in human NK and T cells. *Journal of Immunology (Baltimore, Md.: 1950)*, *165*(4), 1933–1938. https://doi.org/10.4049/jimmunol.165.4.1933

32. Born, T. L., Thomassen, E., Bird, T. A., & Sims, J. E. (1998). Cloning of a Novel Receptor Subunit, AcPL, Required for Interleukin-18 Signaling *. *Journal of Biological Chemistry*, *273*(45), 29445–29450. https://doi.org/10.1074/jbc.273.45.29445

33. Kato, Z., Jee, J., Shikano, H., Mishima, M., Ohki, I., Ohnishi, H., Li, A., Hashimoto, K., Matsukuma, E., Omoya, K., & others. (2003). The structure and binding mode of interleukin-18. *Nature Structural & Molecular Biology*, *10*(11), 966–971.

34. Dinarello, C. A. (1998). Interleukin-1, interleukin-1 receptors and interleukin-1 receptor antagonist. *International Reviews of Immunology*, *16*(5–6), 457–499. https://doi.org/10.3109/08830189809043005

35. Adachi, O., Kawai, T., Takeda, K., Matsumoto, M., Tsutsui, H., Sakagami, M., Nakanishi, K., & Akira, S. (1998). Targeted disruption of the MyD88 gene results in loss of IL-1- and IL-18-mediated function. *Immunity*, *9*(1), 143–150. https://doi.org/10.1016/s1074-7613(00)80596-8

36. Robinson, D., Shibuya, K., Mui, A., Zonin, F., Murphy, E., Sana, T., Hartley, S. B., Menon, S., Kastelein, R., Bazan, F., & O'Garra, A. (1997). IGIF does not drive Th1 development but synergizes with IL-12 for interferon-gamma production and activates IRAK and NFkappaB. *Immunity*, *7*(4), 571–581. https://doi.org/10.1016/s1074-7613(00)80378-7

37. Kalina, U., Kauschat, D., Koyama, N., Nuernberger, H., Ballas, K., Koschmieder, S., Bug, G., Hofmann, W. K., Hoelzer, D., & Ottmann, O. G. (2000). IL-18 activates STAT3 in the natural killer cell line 92, augments cytotoxic activity, and mediates IFN-gamma production by the stress kinase p38 and by the extracellular regulated kinases p44erk-1 and p42erk-21. *Journal of Immunology (Baltimore, Md.: 1950)*, *165*(3), 1307–1313. https://doi.org/10.4049/jimmunol.165.3.1307

38. Yun, W., & Li, C. (2010). JNK pathway is required for TNCB-induced IL-18 expression in murine keratinocytes. *Toxicology in Vitro: An International Journal Published in Association with BIBRA*, *24*(4), 1064–1069. https://doi.org/10.1016/j.tiv.2010.04.001

39. Song, H., Kim, K.-E., Hur, D., Lim, J.-S., Yang, Y., Cho, B. J., Kim, C.-H., Kim, T., Bang, S., Lee, W. J., Park, H., & Cho, D. (2008). IL-18 enhances ULBP2 expression through the MAPK pathway in leukemia cells. *Immunology Letters*, *120*(1–2), 103–107. https://doi.org/10.1016/j.imlet.2008.07.007

40. Chaix, J., Tessmer, M. S., Hoebe, K., Fuséri, N., Ryffel, B., Dalod, M., Alexopoulou, L., Beutler, B., Brossay, L., Vivier, E., & Walzer, T. (2008). Cutting edge: Priming of NK cells by IL-18. *Journal of Immunology (Baltimore, Md.: 1950)*, *181*(3), 1627–1631. https://doi.org/10.4049/jimmunol.181.3.1627

41. Becker-Hapak, M. K., Shrestha, N., McClain, E., Dee, M. J., Chaturvedi, P., Leclerc, G. M., Marsala, L. I., Foster, M., Schappe, T., Tran, J., Desai, S., Neal, C. C., Pence, P., Wong, P., Wagner, J. A., Russler-Germain, D. A., Zhu, X., Spanoudis, C. M., Gallo, V. L., … Fehniger, T. A. (2021). A Fusion Protein Complex that Combines IL-12, IL-15, and IL-18 Signaling to Induce Memory-Like NK Cells for Cancer Immunotherapy. *Cancer Immunology Research*, *9*(9), 1071–1087. https://doi.org/10.1158/2326-6066.CIR-20-1002

42. Boieri, M., Ulvmoen, A., Sudworth, A., Lendrem, C., Collin, M., Dickinson, A. M., Kveberg, L., & Inngjerdingen, M. (2017). IL-12, IL-15, and IL-18 pre-activated NK cells target resistant T cell acute lymphoblastic leukemia and delay leukemia development in vivo. *Oncoimmunology*, *6*(3), e1274478. https://doi.org/10.1080/2162402X.2016.1274478

43. Terrén, I., Orrantia, A., Mosteiro, A., Vitallé, J., Zenarruzabeitia, O., & Borrego, F. (2021). Metabolic changes of Interleukin-12/15/18-stimulated human NK cells. *Scientific Reports*, *11*(1), Article 1. https://doi.org/10.1038/s41598-021-85960-6

44. Coma, G., Peña, R., Blanco, J., Rosell, A., Borras, F. E., Esté, J. A., Clotet, B., Ruiz, L., Parkhouse, R. M. E., & Bofill, M. (2006). Treatment of monocytes with interleukin (IL)-12 plus IL-18 stimulates survival, differentiation and the production of CXC chemokine ligands (CXCL)8, CXCL9 and CXCL10. *Clinical and Experimental Immunology*, *145*(3), 535–544. https://doi.org/10.1111/j.1365-2249.2006.03145.x

45. Schindler, H., Lutz, M. B., Röllinghoff, M., & Bogdan, C. (2001). The production of IFN-gamma by IL-12/IL-18-activated macrophages requires STAT4 signaling and is inhibited by IL-4. *Journal of Immunology (Baltimore, Md.: 1950)*, *166*(5), 3075–3082. https://doi.org/10.4049/jimmunol.166.5.3075

46. Nakanishi, K. (2018). Unique Action of Interleukin-18 on T Cells and Other Immune Cells. *Frontiers in Immunology*, *9*, 763. https://doi.org/10.3389/fimmu.2018.00763

47. Yoshimoto, T., Okamura, H., Tagawa, Y. I., Iwakura, Y., & Nakanishi, K. (1997). Interleukin 18 together with interleukin 12 inhibits IgE production by induction of interferon-gamma production from activated B cells. *Proceedings of the National Academy of Sciences of the United States of America*, *94*(8), 3948–3953. https://doi.org/10.1073/pnas.94.8.3948

48. Hoshino, T., Wiltrout, R. H., & Young, H. A. (1999). IL-18 is a potent coinducer of IL-13 in NK and T cells: A new potential role for IL-18 in modulating the immune response. *Journal of Immunology (Baltimore, Md.: 1950)*, *162*(9), 5070–5077.

49. Ueno, N., Kashiwamura, S.-I., Ueda, H., Okamura, H., Tsuji, N. M., Hosohara, K., Kotani, J., & Marukawa, S. (2005). Role of interleukin 18 in nitric oxide production and pancreatic damage during acute pancreatitis. *Shock (Augusta, Ga.)*, *24*(6), 564–570. https://doi.org/10.1097/01.shk.0000184285.57375.bc

50. Ohtsuki, T., Micallef, M. J., Kohno, K., Tanimoto, T., Ikeda, M., & Kurimoto, M. (1997). Interleukin 18 enhances Fas ligand expression and induces apoptosis in Fas-expressing human myelomonocytic KG-1 cells. *Anticancer Research*, *17*(5A), 3253–3258.

51. Jablonska, E., & Jablonski, J. (2002). Effect of IL-18 on the release of IL-6 and its soluble receptors: SIL-6Ralpha and sgp130 by human neutrophils. *Immunological Investigations*, *31*(3–4), 159–167. https://doi.org/10.1081/imm-120016237

52. Carbotti, G., Barisione, G., Orengo, A. M., Brizzolara, A., Airoldi, I., Bagnoli, M., Pinciroli, P., Mezzanzanica, D., Centurioni, M. G., Fabbi, M., & Ferrini, S. (2013). The IL-18 Antagonist IL-18–Binding Protein Is Produced in the Human Ovarian Cancer Microenvironment. *Clinical Cancer Research*, *19*(17), 4611–4620. https://doi.org/10.1158/1078-0432.CCR-13-0568

53. Tsutsumi, N., Kimura, T., Arita, K., Ariyoshi, M., Ohnishi, H., Yamamoto, T., Zuo, X., Maenaka, K., Park, E. Y., Kondo, N., Shirakawa, M., Tochio, H., & Kato, Z. (2014). The structural basis for receptor recognition of human interleukin-18. *Nature Communications*, *5*(1), 5340. https://doi.org/10.1038/ncomms6340

54. Nold-Petry, C. A., Lo, C. Y., Rudloff, I., Elgass, K. D., Li, S., Gantier, M. P., Lotz-Havla, A. S., Gersting, S. W., Cho, S. X., Lao, J. C., Ellisdon, A. M., Rotter, B., Azam, T., Mangan, N. E., Rossello, F. J., Whisstock, J. C., Bufler, P., Garlanda, C., Mantovani, A., … Nold, M. F.

(2015). IL-37 requires the receptors IL-18Rα and IL-1R8 (SIGIRR) to carry out its multifaceted anti-inflammatory program upon innate signal transduction. *Nature Immunology*, *16*(4), 354–365. https://doi.org/10.1038/ni.3103

55. Li, S., Neff, C. P., Barber, K., Hong, J., Luo, Y., Azam, T., Palmer, B. E., Fujita, M., Garlanda, C., Mantovani, A., Kim, S., & Dinarello, C. A. (2015). Extracellular forms of IL-37 inhibit innate inflammation in vitro and in vivo but require the IL-1 family decoy receptor IL-1R8. *Proceedings of the National Academy of Sciences of the United States of America*, *112*(8), 2497–2502. https://doi.org/10.1073/pnas.1424626112

56. Novick, D., Kim, S.-H., Fantuzzi, G., Reznikov, L. L., Dinarello, C. A., & Rubinstein, M. (1999). Interleukin-18 Binding Protein: A Novel Modulator of the Th1 Cytokine Response. *Immunity*, *10*(1), 127–136. https://doi.org/10.1016/S1074-7613(00)80013-8

57. Es, W., C, G.-G., D, H., Aa, de J., Z, T., J, P., Ej, S., D, F., Aa, G., S, A., S, E., T, H., R, G.-M., C, G., & Sw, C. (2018). Interleukin-18 diagnostically distinguishes and pathogenically promotes human and murine macrophage activation syndrome. *Blood*, *131*(13). https://doi.org/10.1182/blood-2017-12-820852

58. Girard, C., Rech, J., Brown, M., Allali, D., Roux-Lombard, P., Spertini, F., Schiffrin, E. J., Schett, G., Manger, B., Bas, S., Del Val, G., & Gabay, C. (2016). Elevated serum levels of free interleukin-18 in adult-onset Still's disease. *Rheumatology (Oxford, England)*, *55*(12), 2237–2247. https://doi.org/10.1093/rheumatology/kew300

59. Girard-Guyonvarc'h, C., Harel, M., & Gabay, C. (2022). The Role of Interleukin 18/Interleukin 18-Binding Protein in Adult-Onset Still's Disease and Systemic Juvenile Idiopathic Arthritis. *Journal of Clinical Medicine*, *11*(2), 430. https://doi.org/10.3390/jcm11020430

60. Hurgin, V., Novick, D., & Rubinstein, M. (2002). The promoter of IL-18 binding protein: Activation by an IFN-γ-induced complex of IFN regulatory factor 1 and CCAAT/enhancer binding protein β. *Proceedings of the National Academy of Sciences*, *99*(26), 16957–16962. https://doi.org/10.1073/pnas.262663399

61. Paulukat, J., Bosmann, M., Nold, M., Garkisch, S., Kämpfer, H., Frank, S., Raedle, J., Zeuzem, S., Pfeilschifter, J., & Mühl, H. (2001). Expression and Release of IL-18 Binding Protein in Response to IFN-γ1. *The Journal of Immunology*, *167*(12), 7038–7043. https://doi.org/10.4049/jimmunol.167.12.7038

62. Mühl, H., Kämpfer, H., Bosmann, M., Frank, S., Radeke, H., & Pfeilschifter, J. (2000). Interferon-gamma mediates gene expression of IL-18 binding protein in nonleukocytic cells. *Biochemical and Biophysical Research Communications*, *267*(3), 960–963. https://doi.org/10.1006/bbrc.1999.2064

63. Corbaz, A., ten Hove, T., Herren, S., Graber, P., Schwartsburd, B., Belzer, I., Harrison, J., Plitz, T., Kosco-Vilbois, M. H., Kim, S.-H., Dinarello, C. A., Novick, D., van Deventer, S., & Chvatchko, Y. (2002). IL-18-Binding Protein Expression by Endothelial Cells and Macrophages Is Up-Regulated During Active Crohn's Disease1. *The Journal of Immunology*, *168*(7), 3608–3616. https://doi.org/10.4049/jimmunol.168.7.3608

64. Marotte, H., Ahmed, S., Ruth, J. H., & Koch, A. E. (2010). Blocking ERK-1/2 reduces tumor necrosis factor α–induced interleukin-18 bioactivity in rheumatoid arthritis synovial fibroblasts by induction of interleukin-18 binding protein A. *Arthritis & Rheumatism*, *62*(3), 722–731. https://doi.org/10.1002/art.27269

65. Wittmann, M., Doble, R., Bachmann, M., Pfeilschifter, J., Werfel, T., & Mühl, H. (2012). IL-27 Regulates IL-18 Binding Protein in Skin Resident Cells. *PLOS ONE*, *7*(6), e38751. https://doi.org/10.1371/journal.pone.0038751

66. Gracie, J. A., Forsey, R. J., Chan, W. L., Gilmour, A., Leung, B. P., Greer, M. R., Kennedy, K., Carter, R., Wei, X. Q., Xu, D., Field, M., Foulis, A., Liew, F. Y., & McInnes, I. B. (1999). A proinflammatory role for IL-18 in rheumatoid arthritis. *The Journal of Clinical Investigation*, *104*(10), 1393–1401. https://doi.org/10.1172/JCI7317

67. Losy, J., & Niezgoda, A. (2001). IL-18 in patients with multiple sclerosis. *Acta Neurologica Scandinavica*, *104*(3), 171–173. https://doi.org/10.1034/j.1600-0404.2001.00356.x

68. Harms, R. Z., Yarde, D. N., Guinn, Z., Lorenzo-Arteaga, K. M., Corley, K. P., Cabrera, M. S., & Sarvetnick, N. E. (2015). Increased expression of IL-18 in the serum and islets of type 1 diabetics. *Molecular Immunology*, *64*(2), 306–312. https://doi.org/10.1016/j.molimm.2014.12.012

69. Stone, D. L., Ombrello, A., Arostegui, J. I., Schneider, C., Dang, V., de Jesus, A., Girard-Guyonvarc'h, C., Gabay, C., Lee, W., Chae, J. J., Aksentijevich, I., Goldbach-Mansky, R. T., Kastner, D. L., & Canna, S. W. (2022). Excess Serum Interleukin-18 Distinguishes Patients With Pathogenic Mutations in PSTPIP1. *Arthritis & Rheumatology (Hoboken, N.J.)*, *74*(2), 353–357. https://doi.org/10.1002/art.41976

70. Yasin, S., Fall, N., Brown, R. A., Henderlight, M., Canna, S. W., Girard-Guyonvarc'h, C., Gabay, C., Grom, A. A., & Schulert, G. S. (2019). IL-18 as a biomarker linking systemic juvenile idiopathic arthritis and macrophage activation syndrome. *Rheumatology (Oxford, England)*, *59*(2), 361–366. https://doi.org/10.1093/rheumatology/kez282

71. Krei, J. M., Møller, H. J., & Larsen, J. B. (2021). The role of interleukin-18 in the diagnosis and monitoring of hemophagocytic lymphohistiocytosis/macrophage activation syndrome – a systematic review. *Clinical and Experimental Immunology*, *203*(2), 174–182. https://doi.org/10.1111/cei.13543

72. Weiss, E. S., Girard-Guyonvarc'h, C., Holzinger, D., de Jesus, A. A., Tariq, Z., Picarsic, J., Schiffrin, E. J., Foell, D., Grom, A. A., Ammann, S., Ehl, S., Hoshino, T., Goldbach-Mansky, R., Gabay, C., & Canna, S. W. (2018). Interleukin-18 diagnostically distinguishes and pathogenically promotes human and murine macrophage activation syndrome. *Blood*, *131*(13), 1442–1455. https://doi.org/10.1182/blood-2017-12-820852

73. Krumm, B., Meng, X., Wang, Z., Xiang, Y., & Deng, J. (2012). A Unique Bivalent Binding and Inhibition Mechanism by the Yatapoxvirus Interleukin 18 Binding Protein. *PLoS Pathogens*, *8*(8), e1002876. https://doi.org/10.1371/journal.ppat.1002876

74. Wei, H., Wang, D., Qian, Y., Liu, X., Fan, S., Yin, H.-S., & Wang, X. (2014). Structural basis for the specific recognition of IL-18 by its alpha receptor. *FEBS Letters*, *588*(21), 3838–3843. https://doi.org/10.1016/j.febslet.2014.09.019

75. Krumm, B., Meng, X., Li, Y., Xiang, Y., & Deng, J. (2008). Structural basis for antagonism of human interleukin 18 by poxvirus interleukin 18-binding protein. *Proceedings of the National Academy of Sciences of the United States of America*, *105*(52), 20711–20715. https://doi.org/10.1073/pnas.0809086106

76. Detry, S., Andries, J., Bloch, Y., Gabay, C., Clancy, D. M., & Savvides, S. N. (2022). Structural basis of human IL-18 sequestration by the decoy receptor IL-18 binding protein in inflammation and tumor immunity. *Journal of Biological Chemistry*, *298*(5). https://doi.org/10.1016/j.jbc.2022.101908

77. Krumm, B., Meng, X., Xiang, Y., & Deng, J. (2017). Identification of small molecule inhibitors of Interleukin-18. *Scientific Reports*, *7*(1), 483. https://doi.org/10.1038/s41598-017-00532-x

78. Krumm, B., Meng, X., Xiang, Y., & Deng, J. (2015). Crystallization of interleukin-18 for structure-based inhibitor design. *Acta Crystallographica Section F: Structural Biology Communications*, *71*(6), 710–717. https://doi.org/10.1107/S2053230X15006871

79. Eswar, N., Eramian, D., Webb, B., Shen, M.-Y., & Sali, A. (2008). Protein structure modeling with MODELLER. *Methods in Molecular Biology (Clifton, N.J.)*, *426*, 145–159. https://doi.org/10.1007/978-1-60327-058-8_8

80. Marti-Renom, M. A., Yerkovich, B., & Sali, A. (2002). Comparative Protein Structure Prediction. *Current Protocols in Protein Science*, *28*(1), 2.9.1-2.9.22. https://doi.org/10.1002/0471140864.ps0209s28

81. Kozakov, D., Hall, D. R., Xia, B., Porter, K. A., Padhorny, D., Yueh, C., Beglov, D., & Vajda, S. (2017). The ClusPro web server for protein-protein docking. *Nature Protocols*, *12*(2), 255–278. https://doi.org/10.1038/nprot.2016.169

82. van Zundert, G. C. P., Rodrigues, J. P. G. L. M., Trellet, M., Schmitz, C., Kastritis, P. L., Karaca, E., Melquiond, A. S. J., van Dijk, M., de Vries, S. J., & Bonvin, A. M. J. J. (2016). The HADDOCK2.2 Web Server: User-Friendly Integrative Modeling of Biomolecular Complexes. *Journal of Molecular Biology*, *428*(4), 720–725. https://doi.org/10.1016/j.jmb.2015.09.014

83. Jumper, J., Evans, R., Pritzel, A., Green, T., Figurnov, M., Ronneberger, O., Tunyasuvunakool, K., Bates, R., Žídek, A., Potapenko, A., Bridgland, A., Meyer, C., Kohl, S. A. A., Ballard, A. J., Cowie, A., Romera-Paredes, B., Nikolov, S., Jain, R., Adler, J., … Hassabis, D. (2021). Highly accurate protein structure prediction with AlphaFold. *Nature*, *596*(7873), 583–589. https://doi.org/10.1038/s41586-021-03819-2

84. Baek, M., DiMaio, F., Anishchenko, I., Dauparas, J., Ovchinnikov, S., Lee, G. R., Wang, J., Cong, Q., Kinch, L. N., Schaeffer, R. D., Millán, C., Park, H., Adams, C., Glassman, C. R., DeGiovanni, A., Pereira, J. H., Rodrigues, A. V., van Dijk, A. A., Ebrecht, A. C., … Baker, D. (2021). Accurate prediction of protein structures and interactions using a three-track neural network. *Science*, *373*(6557), 871–876. https://doi.org/10.1126/science.abj8754

85. Mirdita, M., Schütze, K., Moriwaki, Y., Heo, L., Ovchinnikov, S., & Steinegger, M. (2022). ColabFold: Making protein folding accessible to all. *Nature Methods*, *19*(6), 679–682. https://doi.org/10.1038/s41592-022-01488-1

86. Mirdita, M., Steinegger, M., & Söding, J. (2019). MMseqs2 desktop and local web server app for fast, interactive sequence searches. *Bioinformatics (Oxford, England)*, *35*(16), 2856–2858. https://doi.org/10.1093/bioinformatics/bty1057

87. Steinegger, M., & Söding, J. (2017). MMseqs2 enables sensitive protein sequence searching for the analysis of massive data sets. *Nature Biotechnology*, *35*(11), 1026–1028. https://doi.org/10.1038/nbt.3988

88. Suzek, B. E., Wang, Y., Huang, H., McGarvey, P. B., Wu, C. H., & the UniProt Consortium. (2015). UniRef clusters: A comprehensive and scalable alternative for improving sequence similarity searches. *Bioinformatics*, *31*(6), 926–932. https://doi.org/10.1093/bioinformatics/btu739

89. Steinegger, M., Mirdita, M., & Söding, J. (2019). Protein-level assembly increases protein sequence recovery from metagenomic samples manyfold. *Nature Methods*, *16*(7), 603–606. https://doi.org/10.1038/s41592-019-0437-4

90. Eastman, P., Swails, J., Chodera, J. D., McGibbon, R. T., Zhao, Y., Beauchamp, K. A., Wang, L.-P., Simmonett, A. C., Harrigan, M. P., Stern, C. D., Wiewiora, R. P., Brooks, B. R., & Pande, V. S. (2017). OpenMM 7: Rapid development of high performance algorithms for molecular dynamics. *PLOS Computational Biology*, *13*(7), e1005659. https://doi.org/10.1371/journal.pcbi.1005659

91. Lindahl, E., Hess, B., & van der Spoel, D. (2001). GROMACS 3.0: A package for molecular simulation and trajectory analysis. *Molecular Modeling Annual*, *7*(8), 306–317. https://doi.org/10.1007/s008940100045

92. Abraham, M. J., Murtola, T., Schulz, R., Páll, S., Smith, J. C., Hess, B., & Lindahl, E. (2015). GROMACS: High performance molecular simulations through multi-level parallelism from laptops to supercomputers. *SoftwareX*, *1–2*, 19–25. https://doi.org/10.1016/j.softx.2015.06.001

93. BEKKER, H., BERENDSEN, H., DIJKSTRA, E., ACHTEROP, S., VONDRUMEN, R., VANDERSPOEL, D., SIJBERS, A., Keegstra, H., & RENARDUS, M. (1993). GROMACS - A PARALLEL COMPUTER FOR MOLECULAR-DYNAMICS SIMULATIONS: 4th International Conference on Computational Physics (PC 92). *PHYSICS COMPUTING '92*, 252–256.

94. Van Der Spoel, D., Lindahl, E., Hess, B., Groenhof, G., Mark, A. E., & Berendsen, H. J. C. (2005). GROMACS: Fast, flexible, and free. *Journal of Computational Chemistry*, *26*(16), 1701–1718. https://doi.org/10.1002/jcc.20291

95. Huang, J., & MacKerell Jr, A. D. (2013). CHARMM36 all-atom additive protein force field: Validation based on comparison to NMR data. *Journal of Computational Chemistry*, *34*(25), 2135–2145. https://doi.org/10.1002/jcc.23354

96. Jorgensen, W. L., Chandrasekhar, J., Madura, J. D., Impey, R. W., & Klein, M. L. (1983). Comparison of simple potential functions for simulating liquid water. *The Journal of Chemical Physics*, *79*(2), 926–935. https://doi.org/10.1063/1.445869

97. Darden, T., York, D., & Pedersen, L. (1993). Particle mesh Ewald: An N log(N) method for Ewald sums in large systems. *The Journal of Chemical Physics*, *98*(12), 10089–10092. https://doi.org/10.1063/1.464397

98. Yazıcı, Y. Y., Belkaya, S., & Timucin, E. (2023). A small non-interface surface epitope in human IL18 mediates the dynamics and self-assembly of IL18-IL18BP heterodimers. *Computational and Structural Biotechnology Journal*, *21*, 3522–3531. https://doi.org/10.1016/j.csbj.2023.06.021

99. Humphrey, W., Dalke, A., & Schulten, K. (1996). VMD: Visual molecular dynamics. *Journal of Molecular Graphics*, *14*(1), 33–38. https://doi.org/10.1016/0263-7855(96)00018-5

100. Michaud-Agrawal, N., Denning, E. J., Woolf, T. B., & Beckstein, O. (2011). MDAnalysis: A toolkit for the analysis of molecular dynamics simulations. *Journal of Computational Chemistry*, *32*(10), 2319–2327. https://doi.org/10.1002/jcc.21787

101. Grant, B. J., Rodrigues, A. P. C., ElSawy, K. M., McCammon, J. A., & Caves, L. S. D. (2006). Bio3d: An R package for the comparative analysis of protein structures. *Bioinformatics (Oxford, England)*, *22*(21), 2695–2696. https://doi.org/10.1093/bioinformatics/btl461

102. Kitao, A. (2022). Principal Component Analysis and Related Methods for Investigating the Dynamics of Biological Macromolecules. *J*, *5*(2), Article 2. https://doi.org/10.3390/j5020021

103. Stock, G., Jain, A., Riccardi, L., & Nguyen, P. H. (2012). Exploring the Energy Landscape of Small Peptides and Proteins by Molecular Dynamics Simulations. In *Protein and Peptide Folding, Misfolding, and Non-Folding* (pp. 55–77). John Wiley & Sons, Ltd. https://doi.org/10.1002/9781118183373.ch2

104. Vangone, A., & Bonvin, A. M. (2015). Contacts-based prediction of binding affinity in protein–protein complexes. *ELife*, *4*, e07454. https://doi.org/10.7554/eLife.07454

105. Zhai, L., Feng, L., Xia, L., Yin, H., & Xiang, S. (2016). Crystal structure of glycogen debranching enzyme and insights into its catalysis and disease-causing mutations. *Nature Communications*, *7*(1), Article 1. https://doi.org/10.1038/ncomms11229

106. Rodrigues, J. P. G. L. M., Karaca, E., & Bonvin, A. M. J. J. (2015). Information-Driven Structural Modelling of Protein–Protein Interactions. In A. Kukol (Ed.), *Molecular Modeling of Proteins* (pp. 399–424). Springer. https://doi.org/10.1007/978-1-4939-1465-4_18

107. Shehata, M., Unlu, A., Iglesias-Fernandez, J., Osuna, S., Sezerman, U., & Timucin, E. (2022). *Brave New Surfactant World Revisited by Thermoalkalophilic Lipases: SDS as a Potential Substrate Analog*. ChemRxiv. https://doi.org/10.26434/chemrxiv-2022-wvp9c

108. Rose, G. D., Geselowitz, A. R., Lesser, G. J., Lee, R. H., & Zehfus, M. H. (1985). Hydrophobicity of amino acid residues in globular proteins. *Science (New York, N.Y.)*, *229*(4716), 834–838. https://doi.org/10.1126/science.4023714

109. Tien, M. Z., Meyer, A. G., Sydykova, D. K., Spielman, S. J., & Wilke, C. O. (2013). Maximum Allowed Solvent Accessibilites of Residues in Proteins. *PLoS ONE*, *8*(11), e80635. https://doi.org/10.1371/journal.pone.0080635

110. Miller, S., Janin, J., Lesk, A. M., & Chothia, C. (1987). Interior and surface of monomeric proteins. *Journal of Molecular Biology*, *196*(3), 641–656. https://doi.org/10.1016/0022-2836(87)90038-6

111. Bakan, A., & Bahar, I. (2009). The intrinsic dynamics of enzymes plays a dominant role in determining the structural changes induced upon inhibitor binding. *Proceedings of the National Academy of Sciences*, *106*(34), 14349–14354.

112. Ruff, K. M., & Pappu, R. V. (2021). AlphaFold and implications for intrinsically disordered proteins. *Journal of Molecular Biology*, *433*(20), 167208.

113. Necci, M., Piovesan, D., & Tosatto, S. C. (2021). Critical assessment of protein intrinsic disorder prediction. *Nature Methods*, *18*(5), 472–481.

114. Liu, J., & Nussinov, R. (2016). Allostery: An overview of its history, concepts, methods, and applications. *PLoS Computational Biology*, *12*(6), e1004966.

115. Kuttner, Y. Y., Nagar, T., & Engel, S. (2013). Surface dynamics in allosteric regulation of protein-protein interactions: Modulation of calmodulin functions by Ca2+. *PLoS Computational Biology*, *9*(4), e1003028.

116. Monod, J. (1965). On the nature of allosteric transitions: A plausible model. *Journal of Molecular Biology*, *12*, 88.

117. Hamelberg, D., Mongan, J., & McCammon, J. A. (2004). Accelerated molecular dynamics: A promising and efficient simulation method for biomolecules. *The Journal of Chemical Physics*, *120*(24), 11919–11929.

118. Miao, Y., Feher, V. A., & McCammon, J. A. (2015). Gaussian accelerated molecular dynamics: Unconstrained enhanced sampling and free energy calculation. *Journal of Chemical Theory and Computation*, *11*(8), 3584–3595.

119. Wong, J. W., Ho, S. Y., & Hogg, P. J. (2011). Disulfide bond acquisition through eukaryotic protein evolution. *Molecular Biology and Evolution*, *28*(1), 327–334.

120. Butera, D., Cook, K. M., Chiu, J., Wong, J. W., & Hogg, P. J. (2014). Control of blood proteins by functional disulfide bonds. *Blood, The Journal of the American Society of Hematology*, *123*(13), 2000–2007.

121. Nuara, A. A., Walter, L. J., Logsdon, N. J., Yoon, S. I., Jones, B. C., Schriewer, J. M., Buller, R. M., & Walter, M. R. (2008). Structure and mechanism of IFN-γ antagonism by an orthopoxvirus IFN-γ-binding protein. *Proceedings of the National Academy of Sciences*, *105*(6), 1861–1866.

122. Müller, K. M., Arndt, K. M., & Plückthun, A. (1998). Model and simulation of multivalent binding to fixed ligands. *Analytical Biochemistry*, *261*(2), 149–158.

123. Cheong, H. S., Chang, J. S., Park, J. M., & Byun, S. M. (1990). Affinity enhancement of bispecific antibody against two different epitopes in the same antigen. *Biochemical and Biophysical Research Communications*, *173*(3), 795–800.

APPENDIX

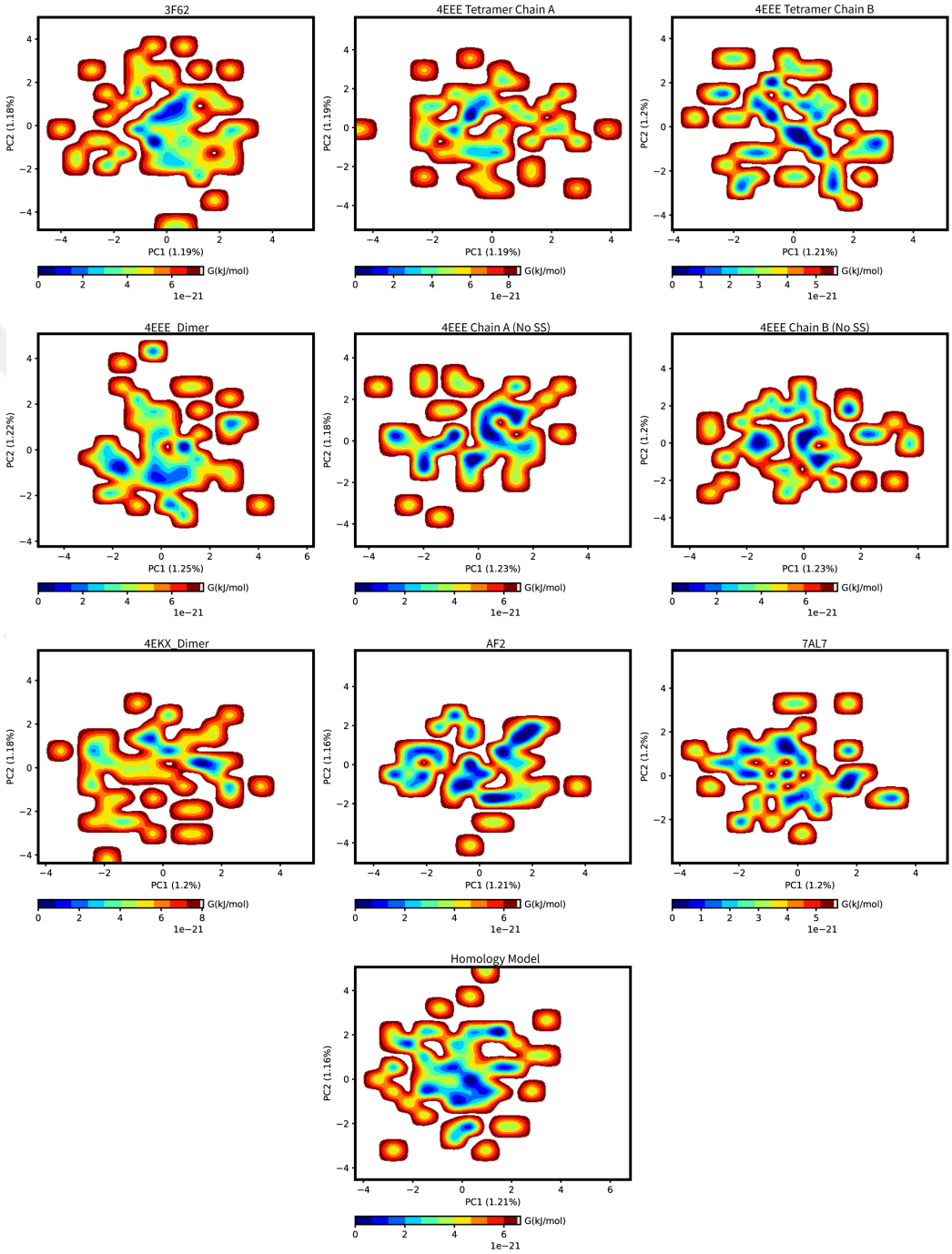

Appendix Figure 1. Essential dynamics and free energy landscape of IL18 by dPCA using cos and sin transformation. Essential dynamics and free energy landscape of IL18 were analyzed by the first two PCs using the cos and sin transformation of the dihedral angle of the last 300 ns of the production run. Possible low-energy conformations can be found in the minimum location in the figure.

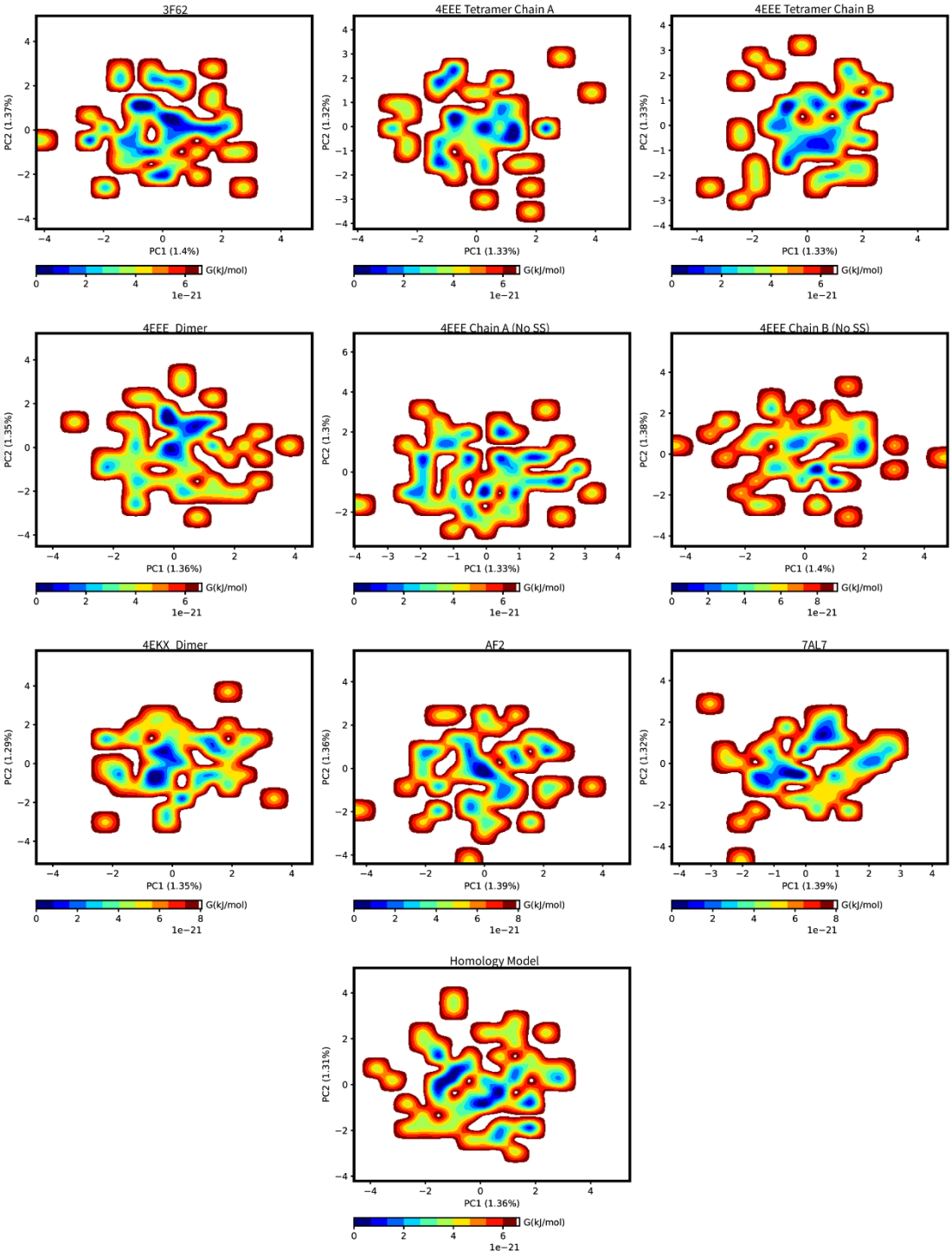

Appendix Figure 2. Essential dynamics and free energy landscape of IL18BP by dPCA using cos and sin transformation. Essential dynamics and free energy landscape of IL18BP were analyzed by the first two PCs using the cos and sin transformation of the dihedral angle of the last 300 ns of the production run. Possible low-energy conformations can be found in the minimum location in the figure.